Available online at www.sciencedirect.com
SCIENCE DIRECT®
Lithos 66 (2003) 173–199
LITHOS
www.elsevier.com/locate/lithos

Accreted fragments of the Late Cretaceous Caribbean–Colombian Plateau in Ecuador

Marc Mamberti[a,b], Henriette Lapierre[b,*], Delphine Bosch[c], Etienne Jaillard[b,d], Raynald Ethien[e], Jean Hernandez[a], Mireille Polvé[f]

[a] *IMP, Université de Lausanne, 1015 Lausanne, Switzerland*
[b] *UMR 5025-CNRS, LGCA, PB 53, 38041 Grenoble Cedex 9, France*
[c] *UMR 5568-CNRS, Tectonophysique, U.M. II, 34095 Montpellier, France*
[d] *IRD, CSS1, 209-213 rue Lafayette, 75840 Paris Cedex 10, France*
[e] *UMR 6524, Université J. Monnet, 42023 St. Etienne Cedex 02, France*
[f] *UMR 5563-CNRS, Univ. P. Sabatier, 38 rue des 36 Ponts, 31400 Toulouse, France*

Received 27 August 2001; accepted 9 September 2002

Abstract

The eastern part of the Western Cordillera of Ecuador includes fragments of an Early Cretaceous (≈ 123 Ma) oceanic plateau accreted around 85–80 Ma (San Juan unit). West of this unit and in fault contact with it, another oceanic plateau sequence (Guaranda unit) is marked by the occurrence of picrites, ankaramites, basalts, dolerites and shallow level gabbros. A comparable unit is also exposed in northwestern coastal Ecuador (Pedernales unit).

Picrites have LREE-depleted patterns, high εNd_i and very low Pb isotopic ratios, suggesting that they were derived from an extremely depleted source. In contrast, the ankaramites and Mg-rich basalts are LREE-enriched and have radiogenic Pb isotopic compositions similar to the Galápagos HIMU component; their εNd_i are slightly lower than those of the picrites. Basalts, dolerites and gabbros differ from the picrites and ankaramites by flat rare earth element (REE) patterns and lower εNd; their Pb isotopic compositions are intermediate between those of the picrites and ankaramites. The ankaramites, Mg-rich basalts, and picrites differ from the lavas from the San Juan–Multitud Unit by higher Pb ratios and lower εNd_i.

The Ecuadorian and Gorgona 88–86 Ma picrites are geochemically similar. The Ecuadorian ankaramites and Mg-rich basalts share with the 92–86 Ma Mg-rich basalts of the Caribbean–Colombian Oceanic Plateau (CCOP) similar trace element and Nd and Pb isotopic chemistry. This suggests that the Pedernales and Guaranda units belong to the Late Cretaceous CCOP. The geochemical diversity of the Guaranda and Pedernales rocks illustrates the heterogeneity of the CCOP plume source and suggests a multi-stage model for the emplacement of these rocks. Stratigraphic and geological relations strongly suggest that the Guaranda unit was accreted in the late Maastrichtian (≈ 68–65 Ma).

Keywords: Oceanic plateaus; Colombian–Caribbean; Western Ecuador; Trace element and radiogenic isotopic geochemistry; High-Mg melts

1. Introduction

The margins of the Caribbean plate and the western margin of northern South America include accreted oceanic sequences (Gansser, 1973), most of which

* Corresponding author. Tel.: +33-4-7663-5906; fax: +33-4-7651-4058.
E-mail address: henriette.lapierre@ujf-grenoble.fr (H. Lapierre).

0024-4937/02/$ - see front matter © 2002 Elsevier Science B.V. All rights reserved.
PII: S0024-4937(02)00218-9

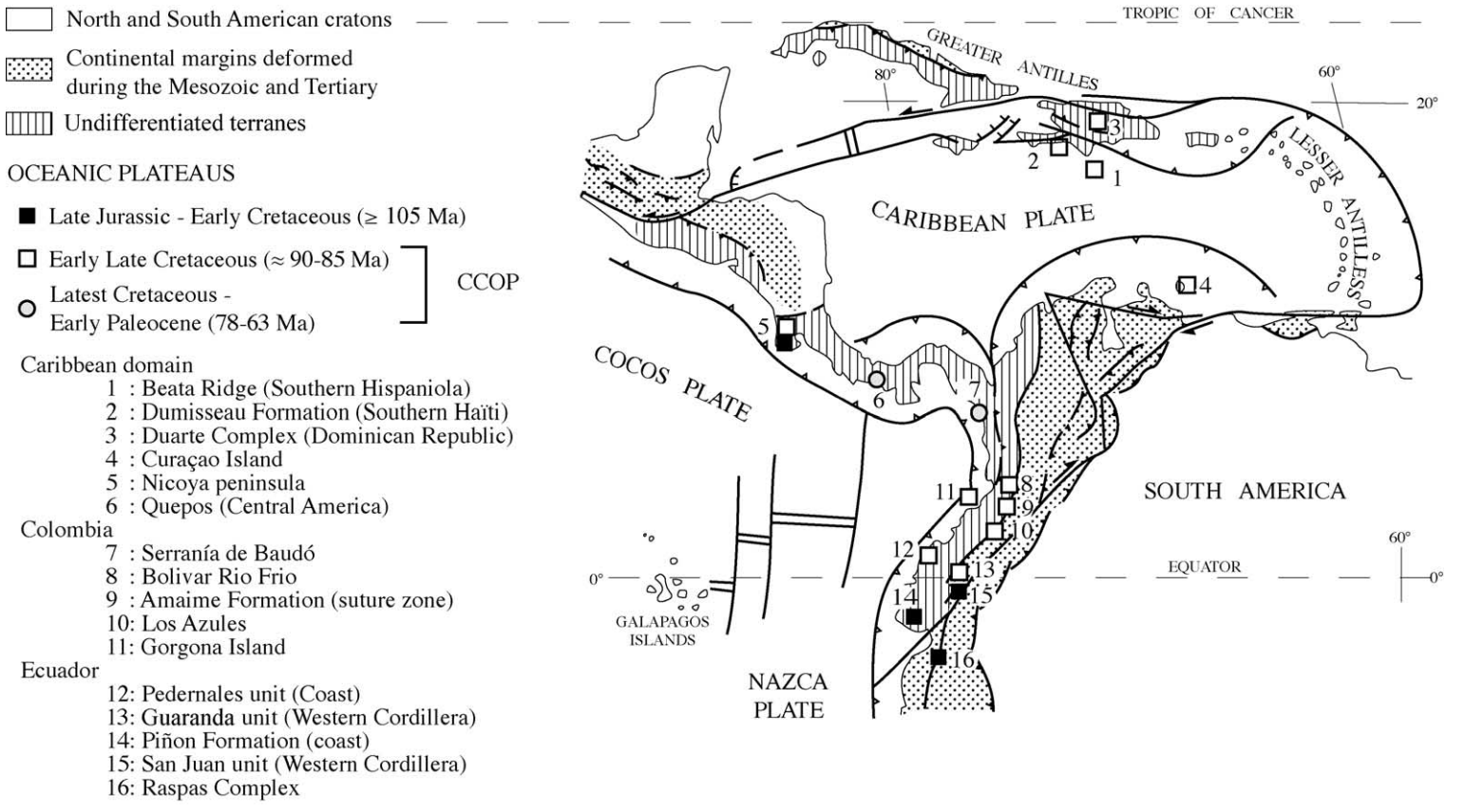

Fig. 1. Schematic map showing the location of the Mesozoic plateau crustal fragments exposed in Costa Rica, Greater Antilles, Curaçao, Colombia, and western Ecuador. The age of the formations are reported after: Beata Ridge after Sinton et al. (1998), Dumisseau Formation after Sen et al. (1988), Duarte Complex after Lapierre et al. (1999), Curaçao Island, Nicoya peninsula and Quepos after Kerr et al. (1997b), all the Colombian Formation after Kerr et al. (1997a) and Sinton et al. (1998), Pedernales unit (this paper), Pallatanga unit after Boland et al. (2000), San Juan unit after Lapierre et al. (2000) and this paper Raspas Complex after Feininger and Bristow (1980).

have oceanic plateau affinity (Fig. 1). These oceanic plateau remnants, however, differ in their petrology, geochemistry and age. It is commonly accepted that oceanic fragments accreted in central America, in the Caribbean islands and in northwestern South America represent remnants of the Late Cretaceous Caribbean–Colombian Oceanic Plateau (CCOP; Donnelly et al., 1990; Kerr et al., 1996a,b; Sinton and Duncan, 1997; Sinton et al., 1998). Three magmatic events have been recognized in the CCOP (Sinton et al., 1998). The oldest of 92–86 Ma age (Turonian–Coniacian) is the most widespread and volumetrically important. A volumetrically secondary and less widespread event occurred at 78–72 Ma (Campanian). This event is known in Coastal Colombia (Serranía del Baudó), Curaçao, Beata Ridge (Révillon et al., 2000a), near the Hess Escarpment and possibly in Haiti. The third event is represented by younger OIB-type basalts of 63 Ma (Paleocene) outcropping in the Quepos Peninsula (Costa Rica, Hauff et al., 1997). Moreover, among all the best-known oceanic plateaus of Mesozoic age, the CCOP is the only one where komatiites have been described and studied (Aitken and Echeverria, 1984; Arndt et al., 1997; Révillon et al., 2000b). The picritic and komatiitic basalts from Gorgona and Colombia are related to the older and major 92–86 Ma pulse (Sinton and Duncan, 1997; Kerr et al., 1997a, 1997b).

However, northwestern South America also includes oceanic terranes of older ages, accreted between the Late Jurassic and the Late Cretaceous. A Late Jurassic–Early Cretaceous suture, containing metamorphosed oceanic and continental rocks, has been identified in Colombia (McCourt et al., 1984; Aspden and McCourt, 1986; Toussaint and Restrepo, 1994) and in Ecuador (Litherland et al., 1994; Arculus et al., 1999; Gabriele et al., 1999; Bosch et al., 2002). On the other hand, remnants of an Early Cretaceous oceanic plateau, distinct from the CCOP have been recently reported in Ecuador (Reynaud et al., 1999; Lapierre et al., 2000).

In order to understand the genesis and emplacement of the magmatic products related to a mantle plume, and to reconstruct the tectonic and geodynamic history of the buildup of this part of the Andes, we undertook the geochemical survey of the oceanic terranes accreted in western Ecuador.

The main aims of this paper are: (i) to present new trace element and isotope (Sr, Nd Pb) data from the picrites and Mg-rich basalts from the Western Cordillera and coastal zone of northwestern Ecuador; and (ii) to compare these rocks with both the fragments of an Early Cretaceous oceanic plateau exposed in Ecuador and with the 92–86 Ma lavas exposed on different parts of the CCOP.

2. Geological setting

The Coast and Western Cordillera of Ecuador are characterized by the presence of oceanic terranes accreted to the Andean margin between the Late Santonian–Campanian (85–80 Ma) and the Eocene (≈ 40 Ma) (Feininger and Bristow, 1980; Lebrat et al., 1987; Jaillard et al., 1997; Cosma et al., 1998; Hughes et al., 1999; Boland et al., 2000).

2.1. Coastal Ecuador

The coastal zone of Ecuador consists of Cretaceous basalts and dolerites with oceanic plateau affinity (Piñón Formation) overlain by Late Cretaceous island arc rocks (Lebrat et al., 1987; Jaillard et al., 1995; Reynaud et al., 1999). These rocks were formerly known as the Basic Igneous Complex (Goossens and Rose, 1973). Although the age of the Piñón Formation is poorly constrained (K/Ar ages range from 180 to 54 Ma, Goossens and Rose, 1973; Pichler and Aly, 1983; Malone et al., 1999), it is certainly pre-90 Ma, and more probably pre-95 Ma, in southwestern Ecuador (Guayaquil area), since the Piñón Formation is stratigraphically overlain by arc-derived sediments of Turonian (and Cenomanian?) to Campanian age (Cayo Formation, e.g., Jaillard et al., 1995; Reynaud et al., 1999). We have sampled exceptionally preserved olivine-bearing dolerite in the Santa Elena vicinity and poorly exposed basalts, east of Guayaquil.

In the Manta area (Fig. 2), the Piñón Formation is overlain by island arcs rocks and sediments of well-constrained Middle Campanian–Middle Maastrichtian age (San Lorenzo Formation; Lebrat et al., 1987; Romero, 1990; Jaillard et al., 1995; Ordoñez, 1996). This strongly suggests that at least two tectonic units are present in the Coastal area, characterized by

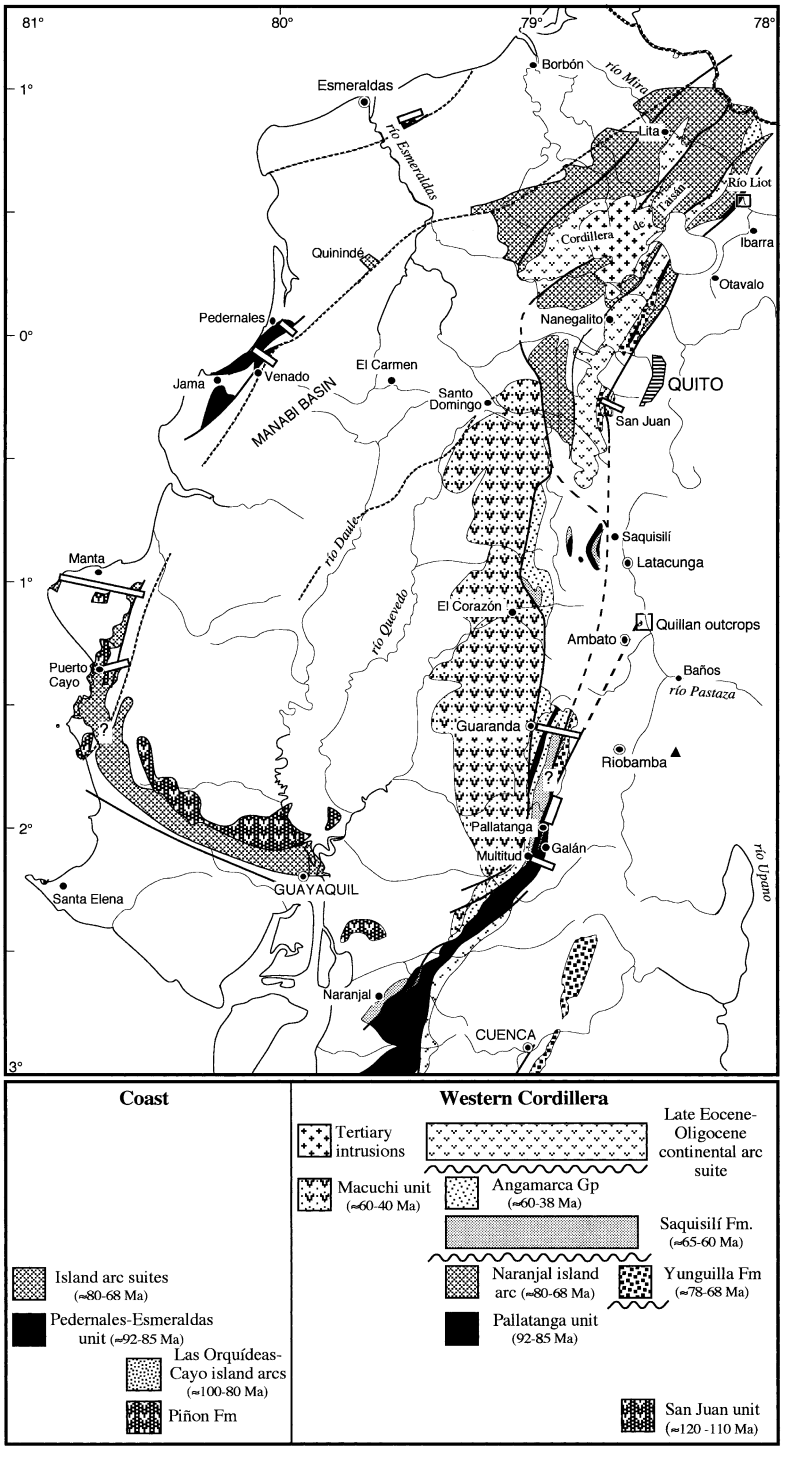

Fig. 2. Schematic geological map of Western Ecuador showing the main geological and tectonic units (after Pratt et al., 1998; Hughes et al., 1999).

oceanic basement rocks and island arcs rocks of distinct ages. The igneous rocks of the Manta area have been studied along two sections, located south of Manta and east of Puerto Cayo, respectively (Fig. 2), and partly published by Reynaud et al. (1999). They consist of pillowed and columnar-joint massive basaltic flows intruded by shallow level doleritic sills and stocks.

In northern coastal Ecuador, we have sampled the oceanic basement in three localities: Esmeraladas, Quininde, and Pedernales. Pedernales and Esmeraldas cross-sections are characterized by hyaloclastites, which contain centimeter-sized rounded glass fragments of basaltic ($7.19>MgO_{wt.\%}>8.91$) and picritic ($MgO_{wt.\%}>20$) compositions. They are associated with pillow basalts, dolerites and isotropic gabbros. Pillow basalts with glassy rims and basaltic hyaloclastites are exposed near Venado (15 km south of Jama; Fig. 2). The relations between the picritic hyaloclastites and the pillow basalts remain unknown. The most continuous section of the basaltic succession ($\sim$ 650 m long) is located along the El Cármen–Pedernales road (Fig. 2). This section consists of pillow basalts interlayered with columnar-joint massive flows. Siliceous sediments occur as pillow matrix. Lava flows dip gently in the southwest and are unconformably overlain by Eocene fine-grained greywackes, cherts and pelites. Dolerites and isotropic gabbros occur as small stocks or dykes crosscutting the lava flows.

Manta, Pedernales and Esmeraldas outcrops are unconformably overlain by Middle Eocene forearc sediments.

2.2. Western Cordillera of Ecuador

Magmatic rocks and the associated Late Cretaceous volcaniclastic sediments of the Western Cordillera were formerly called the Macuchi and Cayo de la Sierra Formations, respectively (Faucher et al., 1971). However, as will be reviewed below, more recent work has revised our understanding of the nature and age of these rocks.

North of Quito, the Western Cordillera comprises rocks of oceanic plateau affinity, dated by Santonian radiolarians (Pallatanga unit), and Campanian–Maastrichtian magmatic and volcano-sedimentary rocks of arc affinity (Boland et al., 2000). These Upper Cretaceous rocks of oceanic plateau and arc-affinities are coeval with the oceanic rocks exposed in the Manta area, from which they constitute the northwestern geological extension (Fig. 2). They suggest that a Santonian oceanic plateau basement, overlain by a Campanian–Maastrichtian island arc, already recognized in southern Colombia (Spadea and Espinosa, 1996) and the Caribbean (Sinton et al., 1998), occur also in the northern Western Cordillera.

South of Quito, the Western Cordillera includes two oceanic units (McCourt et al., 1998; Pratt et al., 1998; Dunkley and Gaibor, 1998; Hughes et al., 1999). To the west, the Late Paleogene–Eocene island arc-lavas and sediments are presently known as the Macuchi unit, whereas to the east, the Pallatanga unit consists of Late Cretaceous volcaniclastic rocks and sediments deposited in an oceanic setting, and Cretaceous oceanic magmatic rocks (Fig. 2). Virtually, no island arc rocks are known within the Pallatanga unit. However some back-arc basin rocks (La Portada Unit) have been recently reported by Kerr et al. (2002).

On the basis of geochemical studies and radiometric dates, an ultramatic cumulate sequence, south of Quito has been recently interpreted as representing remnants of an Early Cretaceous oceanic plateau (Lapierre et al., 2000; Mamberti et al., submitted for publication). A gabbro (97SJ13) of the San Juan section yielded a Sm/Nd isochron of 123 ± 13 Ma (plagioclase, whole rock, amphibole; Lapierre et al., 2000).

In summary, these data suggest that two distinct oceanic basements of Early Cretaceous (123–95 Ma) and Late Cretaceous (85 Ma) ages are exposed in Western Ecuador. Here, we present petrological, geochemical and isotopic data, which support this assumption. Six main sections have been studied. The Guaranda, Pallatanga and Galán sections belong to the Western Cordillera (2°–2°30′ S, Fig. 2), whereas the Manta, Pedernales and Esmeraldas sections are located in the coastal zone of northwestern Ecuador (1°30′ S–1°N, Fig. 2). However, we also present some new geochemical results obtained on rocks from Ambato, Quininde, Santa Elena, and Guayaquil areas (Fig. 2) which will complete the data already published on the Western Cordillera and Coastal Ecuador (Reynaud et al., 1999; Lapierre et al., 2000; Mamberti, 2001; Kerr et al., 2002).

Along the Guaranda cross-section, three rock types have been distinguished on the basis of petrographic observations: pillow basalts, ankaramites and picrites (Fig. 3). The pillow basalts are pinched between the picrites and ankaramites to the west, and to the east, Late Cretaceous and Early Tertiary turbidites and subordinate limestones (Yunguilla Formation and Angamarca Group, McCourt et al., 1998). The picrites and ankaramites occur as a pile (~ 100 m thick) of massive sheeted flows gently dipping to the east. Picrites are located at the base of the section while the ankaramites are present at the top. The thickness of the flows ranges between 1 and 4 m. These flows show evidence of accumulation of clinopyroxene and/or olivine at their base while their tops are highly vesicular. The rounded or flattened up to 4 cm-sized vesicules are filled with calcite in the ankaramites and smectites in the picrites.

The Galán and Pallatanga cross-sections are located in a major dextral transcurrent fault zone. The highly faulted Pallatanga cross-section comprises, to the east, fine-grained tuffs, graywackes, dolerites and aphyric basalts; and to the west, aphyric basalts, and ankaramites associated with pyroxenites and dolerites. The Galán cross-section is composed of massive and pillowed basaltic flows and Mg-rich basalts associated with dolerites.

The Ambato exposure, located near Quillán, was formerly ascribed to the old ‘‘Macuchi Formation’’ of Early Tertiary age (Cotteccia and Zezza, 1969). It

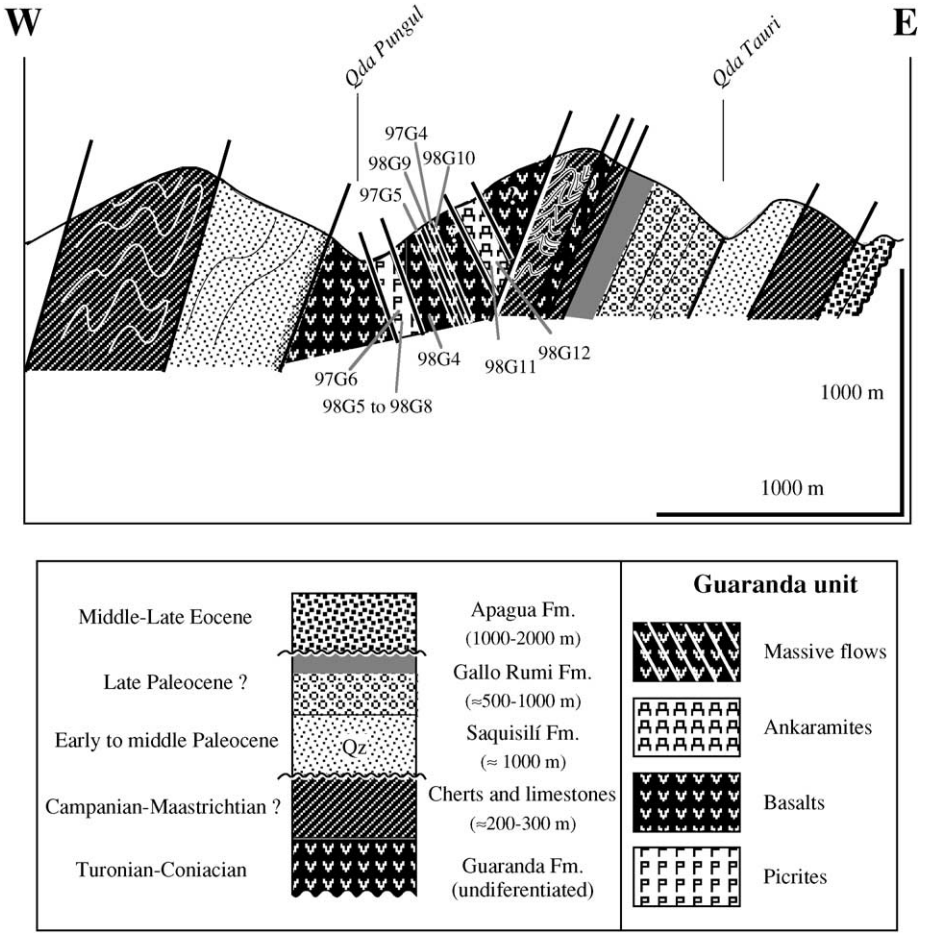

Fig. 3. Schematic Guaranda cross-section showing structural location of the Pallatanga unit, and studied samples.

consists of massive and pillowed basaltic flows overlain by massive dolerites and tuffs. The Ibarra exposure is located on the eastern border of the Western Cordillera of northern Ecuador (río Liot section, 1°N; Fig. 2) and has been mapped by Boland et al. (2000) as the Pallatanga unit. It consists of pillow basalts thrust eastwards upon graywackes.

3. Petrology and mineralogy

3.1. Igneous rocks from northwestern coastal Ecuador

The Manta, Pedernales and Esmeraldas sections and Santa Elena and Guayaquil exposures are composed of hyaloclastites, pillow basalts, dolerites and isotropic gabbros.

The hyaloclastites consist of glass partially replaced by palagonite, which contains centimeter-sized, rounded picritic to basaltic fragments. The basaltic fragments are either composed of plagioclase and clinopyroxene microcrysts enclosed in a more or less altered glassy matrix or are aphyric with preserved glass. Clinopyroxene and plagioclase microcrysts are quenched. The picritic fragments consist of quenched olivine and Cr-spinel enclosed in a preserved glass. The petrology, geochemistry and dating of the picrite will be the subject of a separate paper (Mamberti et al., in preparation).

The pillow basalts are composed of clinopyroxene and plagioclase phenocrysts enclosed in a groundmass formed of abundant quenched plagioclase and clinopyroxene microlites. Plagioclase (up to 0.8 mm long) is altered to albite and exhibits bow-tie and/or dendritic quenched textures. Clinopyroxene clusters into glomeroporphyritic aggregates and is sometimes replaced by calcite (97PE5 and 97PE6). Sample 99PE21 represents the glassy matrix of the pillows.

Massive basalts are aphyric with rare clinopyroxene, olivine (only in 97PE13) and plagioclase phenocrysts. Olivine is completely altered to smectite. Plagioclase is replaced by albite and epidote. The matrix is transformed into smectite and prehnite and locally is crosscut by calcite- and quartz-filled cracks. However, some samples differ by coarser grain size and ophitic texture. In these rocks, clinopyroxene is a magnesian augite (Wo_{43-36}, En_{39-40}, Fs_{10-20}) which shows a Fe-enrichment from core to rim. K_2O very poor plagioclase displays a bytownite composition (An_{85-80}) with Na_2O-enriched rims evolving towards labradorite to andesine. Titano-magnetite and ilmenite are the last minerals to crystallize.

The dolerites and isotropic gabbro exhibit ophitic textures with plagioclase phenocrysts. Most of these rocks consist of millimeter-sized plagioclase laths cemented by clinopyroxene and late crystallizing oxides (magnetite and ilmenite). OLL3 and 97PE14 differ from the other dolerites by the presence of olivine phenocrysts and microcrysts partially or completely replaced by serpentine. Olivine core is a Ni ($\sim 0.1\%$)-poor forsterite (Fo_{73-75}). Clinopyroxene composition ranges from diopside to augite (Wo_{43-46}, En_{43-48}, Fs_{9-12}). When plagioclase is preserved, it has a bytownite and labradorite composition (An_{80-82} and An_{65}, respectively). The late crystallizing oxides fill the space in between the clinopyroxene and plagioclase. 99PE11 gabbro differs from the dolerites by a coarser grain size.

3.2. Igneous rocks from the Western Cordillera

In the Western Cordillera, we have distinguished four types of suites: (1) the Early Cretaceous San Juan ultramafic–mafic cumulate suite, (2) the undated Merced–Multitud pillow basalts, dolerites and gabbroic stocks, (3) the Mg-rich basalts, ankaramites, basalts and dolerites of the Galán–Guaranda–Pallatanga sections, and finally, (4) the Ambato and Ibarra pillow basalts. The petrological and geochemical characteristics of the San Juan suite have been described into a separate paper (Mamberti, 2001; Mamberti et al., submitted for publication).

3.3. Pillow basalts, Mg-rich basalts, ankaramites, dolerites and picrites

Five rock-types have been distinguished on the basis of the field relations, texture, mineralogy and modal compositions. They are the following, listed in decreasing abundance: (1) pillow basalts, (2) Mg-rich basalts, (3) ankaramites, (4) dolerites, and (5) picrites. All the rocks have variably suffered a low-grade hydrothermal alteration. Olivine is totally replaced by serpentine, smectite or calcite. Plagioclase is completely transformed into albite, chlorite or epidote. In

Table 1
Major (wt.%) and trace element (ppm) analyses for the Western Cordillera and Coastal Ecuador samples

Sample	99PE19	99PE20	99PE21	99PE22	97PE5	97PE6	97PE13	99ES1	99ES5	99ES8
Name	Hyaloclastite Basalt	Basalt	Glass	Pillow	Pillow Basalt	Pillow Basalt	Lava Basalt	Hyaloclastite	Hyaloclastite	Dolerite
Locality	Pedernales	Pedernales	Pedernales	Pedernales	Pedernales	Pedernales	Pedernales	Esmeraldas	Esmeraldas	Esmeraldas
SiO_2	52.9	52.3	52.6	51.8	50.3	51.4	51.5	50.9	50.6	50.1
TiO_2	1.34	1.30	1.07	0.99	0.99	1.03	1.16	1.03	1.14	0.92
Al_2O_3	14.1	13.9	14.8	14.6	14.4	14.9	13.3	15.2	15.1	14.3
FeO	12.8	13.1	12.8	10.8	11.1	9.8	11.9	11.7	12.7	11.1
MnO	0.25	0.24	0.31	0.21	0.22	0.18	0.28	0.21	0.23	0.16
MgO	7.40	7.60	7.48	8.73	8.42	7.64	7.79	8.45	8.91	8.69
CaO	8.89	9.29	8.12	10.49	11.24	12.91	11.23	10.70	9.51	12.22
Na_2O	1.33	1.70	2.22	2.15	3.03	1.90	2.29	1.23	0.92	2.04
K_2O	0.87	0.52	0.55	0.22	0.22	0.20	0.55	0.45	0.69	0.30
P_2O_5	0.11	0.11	0.07	0.08	0.07	0.05	0.14	0.08	0.08	0.08
Cr_2O_3	0.01	0.01	0.03	0.03	–	–	–	–	–	–
NiO	0.01	0.01	0.01	0.01	–	–	–	–	–	–
LOI	5.91	4.15	3.69	2.07	3.14	2.13	2.79	4.69	8.12	1.01
Total	100	100	100	100	100	100	100	100	100	100
Ba	468.49	93.45	33.47	7.75		25.9	133	33	996	128
Rb	9.55	4.74	4.70	1.02	2.57	0.82	9.59	7.76	12.45	1.52
Sr	648	247	249	162	166	87	577	448.0	765	103
Ta	0.24	0.24	0.20	0.23	0.22	0.23	0.24	0.20	0.22	0.33
Th	0.23	0.23	0.20	0.19	0.23	0.24	0.21	0.19	0.21	0.17
Zr	58.0	58.3	46.8	46.4	51.1	52.1	55.8	53.33	61	45
Nb	3.39	3.52	3.14	3.08	3.26	3.30	3.75	3.25	3.83	2.94
Y	24.8	25.2	23.3	20.6	21.4	20.4	23.8	20.99	24.7	19.06
Hf	1.60	1.69	1.33	1.36	1.45	1.50	1.58	1.35	1.41	1.27
V	434	420	394	335	–	–	–	363	372	297
Cr	71	76	223	169	–	–	–	394	392	289
Ni	77	76	107	103	–	–	–	130	134	128
Co	43.4	42.1	45.4	43.0	47.0	42.3	46.6	47	54	44
U	0.10	0.08	0.07	0.07	0.13	0.09	0.10	0.06	0.09	0.05
Pb	0.38	0.41	0.48	0.33	0.41	0.55	0.38	0.27	0.59	260
Sc	80	86	101	63	–	–	–	72	91	44
Cu	120	108	76	94	–	–	–	142	139	98
Zn	100	101	85	82	–	–	–	79	82	61
La	2.99	3.03	2.37	2.55	2.67	2.71	2.89	2.65	2.91	2.42
Ce	7.97	8.32	6.46	6.73	7.24	7.37	7.92	7.08	7.72	6.29
Pr	1.28	1.29	1.03	1.06	1.15	1.17	1.25	1.12	1.25	1.03
Nd	6.43	6.48	5.26	5.36	5.90	5.90	6.40	5.87	6.31	5.32
Sm	2.22	2.16	1.81	1.82	1.94	1.95	2.14	2.02	2.15	1.85
Eu	0.86	0.84	0.77	0.69	0.76	0.76	0.83	0.73	0.83	0.68
Gd	3.17	3.12	2.64	2.57	2.66	2.64	2.93	2.69	2.70	2.59
Tb	0.59	0.61	0.52	0.48	0.49	0.48	0.54	0.51	0.53	0.46
Dy	3.85	3.92	3.45	3.21	3.33	3.26	3.66	3.38	3.54	3.22
Ho	0.86	0.90	0.81	0.73	0.74	0.71	0.82	0.79	0.74	0.68
Er	2.56	2.57	2.31	2.10	2.13	2.04	2.36	2.02	2.09	1.85
Tm	–	–	–	–	–	–	–	–	–	–
Yb	2.49	2.51	2.17	2.00	2.02	1.95	2.25	2.08	2.16	1.94
Lu	0.38	0.41	0.35	0.33	0.32	0.31	0.36	0.32	0.34	0.30
$(Ce/Yb)_n$	0.83	0.86	0.77	0.87	0.93	0.98	0.91	0.88	0.92	0.84
$(La/Sm)_n$	0.85	0.89	0.82	0.88	0.87	0.88	0.85	0.83	0.85	0.83
$(La/Yb)_n$	0.81	0.82	0.74	0.86	0.89	0.94	0.86	0.86	0.91	0.84

97G5	97G6	98G5	98G6	98G7	98G8	97G2	99PE11	99PE24	99PE25	97PE14	98G10
Picrite	Picrite	Picrite	Picrite	Picrite	Picrite	Dolerite	Doleritic Gabbro	Dolerite	Dolerite	Dolerite	Ankaramite
Guaranda	Guaranda	Guaranda	Guaranda	Guaranda	Guaranda	Guaranda	Galán	Pedernales	Pedernales	Pedernales	Guaranda
43.7	44.6	44.9	42.9	47.1	44.6	53.6	51.1	49.4	49.6	66.4	49.0
0.78	0.56	0.54	0.83	0.56	0.78	1.47	1.67	0.88	1.08	0.43	1.15
10.2	7.1	7.0	10.8	7.6	10.3	15.3	14.4	14.7	15.8	10.0	12.1
13.5	11.6	11.1	12.1	10.3	11.6	13.6	13.4	10.5	11.1	5.5	11.5
0.21	0.18	0.18	0.20	0.17	0.20	0.19	0.23	0.16	0.19	0.10	0.19
19.85	27.26	27.29	22.21	23.04	21.53	6.25	5.54	8.87	7.20	7.06	10.46
10.87	7.89	8.33	10.05	10.38	10.09	5.30	9.89	13.28	11.84	9.15	11.70
0.39	0.05	0.02	0.24	0.21	0.36	3.88	3.08	1.97	2.81	1.19	3.35
0.05	0.03	0.01	0.01	0.02	0.01	0.23	0.46	0.13	0.22	0.23	0.14
0.09	0.05	0.04	0.06	0.05	0.06	0.12	0.14	0.06	0.09	0.02	0.25
0.24	0.42	0.37	0.43	0.31	0.36	0.02	0.01	0.04	0.01	–	0.08
0.10	0.24	0.23	0.16	0.18	0.13	0.01	0.01	0.02	0.01	–	0.03
5.49	7.10	7.06	5.96	5.32	6.37	7.16	1.92	−0.02	1.99	3.26	1.89
100	100	100	100	100	100	100	100	100	100	100	100
19.9	15.69	5.14	5.68	8.20	5.63	39.2	30.6	19.5	23.9	23.2	49.6
0.77	1.42	1.44	0.60	0.53	0.48	2.74	4.00	1.47	1.22	8.75	0.81
14.6	31.01	25.1	11.6	12.0	11.4	172	118	121	133	139	152
0.07	0.04	0.04	0.06	0.04	0.05	0.24	0.34	0.16	0.21	0.10	0.34
0.05	0.04	0.03	0.04	0.03	0.04	0.26	0.33	0.15	0.21	0.10	0.25
29.5	24.76	22.6	33.4	24.6	32.5	60.0	66.6	38.3	49.2	26.2	58.0
1.63	0.60	0.56	0.80	0.62	0.84	4.06	5.25	2.35	3.08	1.53	7.57
15.0	8.76	8.20	12.2	8.90	12.2	25.5	29.6	18.6	21.5	13.0	17.4
0.88	0.72	0.65	0.96	0.71	0.94	1.66	1.96	1.15	1.40	0.82	1.55
245	193	179	278	196	282	551	411	272	321	–	341
1246	1952	1298	2630	1554	1910	161	35	231	65	–	519
837	1346	1178	867	995	841	87	48	129	87	–	220
100	90.68	88.2	72.9	79.0	74.4	50.4	39.7	49.0	45.1	42.5	60.5
0.02	0.01	0.01	0.01	0.01	0.01	0.12	0.11	0.05	0.07	0.04	0.08
0.39	0.62	0.09	0.09	0.09	0.08	0.37	0.16	0.33	0.44	0.24	0.91
29	25	61	75	65	81	83	54	45	46	–	52
3	–	11	62	48	18	103	16	80	151	–	91
84	72	63	76	62	71	117	58	87	72	–	95
1.12	0.65	0.58	0.87	0.61	0.83	3.63	3.36	2.25	3.56	1.44	3.50
3.59	2.13	2.00	2.99	2.13	2.93	9.94	10.21	6.14	8.73	4.05	8.50
0.68	0.42	0.38	0.57	0.41	0.57	1.60	1.68	0.99	1.32	0.66	1.37
3.90	2.53	2.28	3.44	2.49	3.42	7.94	8.91	4.99	6.30	3.41	7.04
1.53	1.01	0.92	1.36	0.99	1.38	2.70	2.85	1.74	2.09	1.18	2.30
0.57	0.38	0.36	0.57	0.39	0.50	0.96	1.11	0.71	0.81	0.52	0.83
2.06	1.36	1.25	1.87	1.39	1.89	3.10	3.89	2.32	2.75	1.68	2.78
0.37	0.25	0.23	0.34	0.25	0.34	0.64	0.72	0.46	0.51	0.32	0.49
2.36	1.59	1.44	2.15	1.58	2.18	4.26	4.73	2.86	3.35	2.11	3.10
0.50	0.31	0.30	0.46	0.33	0.46	0.92	1.07	0.65	0.74	0.47	0.63
1.39	0.80	0.80	1.20	0.88	1.21	2.48	3.00	1.81	2.11	1.33	1.61
–	–	–	–	–	–	0.40	–	–	–	–	–
1.20	0.75	0.72	1.06	0.78	1.07	2.65	2.85	1.68	1.95	1.27	1.52
0.18	0.11	0.11	0.16	0.12	0.16	0.40	0.44	0.27	0.31	0.19	0.22
0.78	0.73	0.72	0.73	0.71	0.71	0.97	0.93	0.95	1.16	0.83	1.44
0.53	0.41	0.40	0.40	0.39	0.38	0.85	0.74	0.81	1.07	0.77	0.96
0.73	0.58	0.55	0.55	0.53	0.52	0.92	0.80	0.91	1.23	0.77	1.55

(continued on next page)

Table 1 (*continued*)

Sample	98G11	98G12	97G4	98G4	98G9	98P3	98P7	98P8	98P10	99PE15
Name	Ankaramite	Ankaramite	Ankaramite	Ankaramite	Ankaramite	Basalt	Basalt	Basalt	Pillow Basalt	Basalt
Locality	Guaranda	Guaranda	Guaranda	Guaranda	Guaranda	Pallatanga	Galán	Galán	Galán	Pedernales
SiO_2	48.4	43.4	47.6	48.0	46.6	53.4	48.9	50.8	53.0	52.0
TiO_2	1.11	1.38	1.28	1.28	0.98	1.30	0.98	0.92	1.27	1.28
Al_2O_3	11.7	14.6	12.2	11.2	8.89	14.1	14.6	14.1	13.3	14.2
FeO	10.6	12.7	12.6	12.6	12.5	12.0	12.0	11.0	11.7	12.9
MnO	0.18	0.20	0.20	0.19	0.20	0.19	0.20	0.19	0.21	0.20
MgO	9.93	8.47	12.11	12.99	17.44	8.18	9.00	8.95	6.78	7.19
CaO	15.44	18.02	11.26	11.49	12.51	5.93	11.22	10.25	9.49	7.87
Na_2O	2.21	0.81	1.67	1.42	0.42	4.54	2.95	3.54	4.09	0.84
K_2O	0.10	0.10	0.76	0.57	0.03	0.17	0.04	0.08	0.04	3.43
P_2O_5	0.17	0.21	0.10	0.11	0.08	0.10	0.08	0.08	0.11	0.11
Cr_2O_3	0.11	0.05	0.16	0.12	0.23	0.02	0.04	0.04	0.02	0.02
NiO	0.02	0.02	0.06	0.06	0.09	0.01	0.01	0.01	0.01	0.01
LOI	1.34	2.38	2.89	2.57	3.93	2.76	2.56	3.10	2.61	5.76
Total	100	100	100	100	100	100	100	100	100	100
Ba	44.8	16.43	133	116	6.62	47.51	21.72	27.23	16.33	77.79
Rb	0.54	0.68	11.82	7.71	0.51	2.35	0.75	0.71	0.18	20.94
Sr	267	757	85.5	61.8	14.6	128	78.5	86.9	101	205
Ta	0.30	0.40	0.18	0.21	0.27	0.23	0.18	0.24	0.23	0.24
Th	0.23	0.34	0.22	0.25	0.21	0.24	0.18	0.17	0.20	0.22
Zr	54.2	72.0	51.0	69.0	27.1	60.6	49.3	45.1	59.3	56.1
Nb	6.45	9.44	3.22	4.48	3.25	4.34	3.44	3.61	3.51	3.58
Y	17.0	20.6	19.4	17.0	8.25	24.5	20.3	18.1	23.8	23.5
Hf	1.51	1.95	1.48	1.78	0.76	1.72	1.31	1.27	1.71	1.57
V	353	317	355	318	290	437	334	334	418	430
Cr	668	321	989	742	1282	134	243	247	132	111
Ni	167	172	388	400	588	98	109	108	87	75
Co	54.0	57.3	73.9	72.0	75.1	44.5	49.4	43.8	41.2	41.9
U	0.07	0.12	0.08	0.08	0.05	0.08	0.06	0.06	0.08	0.08
Pb	1.51	3.23	0.44	0.27	0.27	0.36	0.32	0.30	0.37	0.39
Sc	52	45	32	55	68	85	74	73	58	75
Cu	217	111	26	18	13	90	63	64	110	106
Zn	83	83	104	94	81	102	90	81	102	98
La	3.57	4.80	3.87	3.69	2.43	3.37	2.57	2.29	2.85	2.89
Ce	8.17	11.11	10.45	10.02	7.01	8.58	6.64	5.90	7.56	7.74
Pr	1.37	1.81	1.62	1.64	1.16	1.36	1.05	0.94	1.23	1.24
Nd	7.13	9.20	7.69	8.54	6.11	7.04	5.42	4.86	6.46	6.25
Sm	2.31	2.89	2.24	2.68	2.02	2.36	1.87	1.63	2.19	2.09
Eu	0.86	1.05	0.85	0.96	0.77	0.90	0.68	0.62	0.74	0.82
Gd	2.81	3.34	2.82	3.16	2.54	3.17	2.50	2.25	3.07	2.90
Tb	0.50	0.59	0.50	0.52	0.45	0.61	0.48	0.43	0.59	0.56
Dy	3.11	3.72	3.19	3.22	2.71	4.17	3.29	2.95	4.10	3.70
Ho	0.63	0.75	0.66	0.63	0.54	0.91	0.72	0.67	0.90	0.83
Er	1.57	1.93	1.79	1.55	1.43	2.43	1.97	1.79	2.51	2.44
Tm	–	–	–	–	–	–	–	–	–	–
Yb	1.47	1.79	1.46	1.36	1.25	2.54	2.08	1.88	2.66	2.37
Lu	0.22	0.26	0.20	0.20	0.18	0.39	0.33	0.30	0.41	0.37
$(Ce/Yb)_n$	1.44	1.60	1.85	1.91	1.45	0.88	0.83	0.81	0.74	0.85
$(La/Sm)_n$	0.98	1.04	1.09	0.87	0.76	0.90	0.86	0.88	0.82	0.87
$(La/Yb)_n$	1.64	1.81	1.79	1.83	1.31	0.90	0.84	0.82	0.73	0.82

99PE16	97G11	97G12	98SL01	97Ma7	97Ma13	97Ma16	97Ma27	99Gy1	99Es12	OLL2	OLL3
Hyaloclastite Basalt	Basalt	Basalt	Basalt	Basalt	Basalt	Basalt	Basalt	Basalt	Dolerite	Dolerite	Dolerite
Pedernales	Quillan	Quillan	San Lorenzo	Montecristi	Montecristi	Puerto Cayo	Puerto Cayo	La Troncal	Quininde	Santa Helena	Santa Helena
52.1	50.23	50.23	50.22	49.90	50.10	50.62	50.34	51.21	50.51	48.91	49.43
0.98	0.87	0.80	1.03	1.25	1.17	1.39	1.33	1.24	0.94	0.96	0.96
14.4	14.69	14.44	14.42	15.12	14.50	16.60	15.92	15.62	14.92	15.17	15.40
10.8	11.22	11.02	12.13	10.81	11.59	10.49	9.37	9.04	10.64	10.09	9.35
0.18	0.16	0.17	0.16	0.16	0.18	0.19	0.15	0.17	0.24	0.15	0.16
8.37	8.31	8.60	7.69	7.87	8.84	6.64	5.37	8.28	8.70	9.17	8.89
11.39	12.89	13.11	12.43	12.64	9.91	11.77	14.07	11.66	11.37	13.53	13.25
1.10	1.55	1.55	1.83	2.09	2.90	2.11	1.94	2.51	2.34	1.83	2.20
0.44	0.00	0.00	0.00	0.00	0.62	0.00	1.35	0.14	0.23	0.08	0.23
0.08	0.08	0.08	0.09	0.15	0.18	0.19	0.15	0.13	0.11	0.10	0.12
0.04	–	–	–	–	–	–	–	–	–	–	–
0.01	–	–	–	–	–	–	–	–	–	–	–
6.05	1.04	1.56	1.86	4.44	5.67	4.07	7.17	2.1	1.32	1.61	2.03
100	100	100	100	100.00	100.00	100.00	100.00	100.00	100.00	100.00	100.00
30.97	14.07	19.81	17.79	12.70	4779	15.00	81.70	9.50	46.00	321.80	214.90
7.44	0.44	1.07	0.72	1.08	7.57	0.54	11.42	1.37	3.28	1.02	2.92
192	85.52	78.62	97.06	98.15	72.80	113.4	106.0	104.1	134.0	171.9	212.9
0.20	0.21	0.19	0.23	0.27	0.24	0.29	0.27	0.13	0.23	0.14	0.18
0.19	0.22	0.23	0.23	0.27	0.21	0.29	0.29	0.12	0.18	0.13	0.19
43.7	47.64	42.43	58.42	67.90	41.15	79.24	70.99	86.99	19.15	32.10	48.18
2.87	3.34	2.96	4.00	4.22	3.74	4.59	4.39	2.23	2.92	2.35	3.02
18.8	20.46	18.49	24.00	25.40	21.59	29.03	26.53	34.86	17.65	17.15	20.36
1.23	1.28	1.21	1.47	1.85	1.28	2.09	1.88	2.09	0.74	0.95	1.30
357	–	–	357	346	315	323	329	302	297	305	294
241	–	–	218	243	225	49	204	334	381	462	379
103	–	–	115	106	106	60	127	92	171	140	133
40.9	–	–	47.5	54.50	48.30	46.60	60.80	45.70	44.80	49.20	48.60
0.05	0.07	0.07	0.07	0.09	0.06	0.09	0.15	0.04	0.05	0.04	0.08
0.30	0.17	0.26	0.27	13.64	8.27	0.38	1.39	0.35	1.6	0.33	0.19
80	–	–	–	–	–	–	–	–	–	–	–
91	–	–	–	–	–	–	–	–	–	–	–
80	–	–	–	–	–	–	–	–	–	–	–
2.36	2.55	2.35	2.92	3.26	3.01	3.75	3.82	2.74	2.28	1.88	2.52
6.27	6.77	6.18	7.74	8.91	7.93	10.3	9.84	8.72	6.05	5.35	7.03
0.98	1.08	0.97	1.23	1.45	1.25	1.68	1.58	1.54	0.98	0.89	1.14
5.05	5.41	5.00	6.26	7.42	6.48	8.72	8.08	8.41	4.94	4.81	5.98
1.70	1.86	1.68	2.10	2.56	2.22	2.92	2.66	3.07	1.69	1.71	2.08
0.66	0.72	0.66	0.80	0.92	0.88	1.09	1.02	1.11	0.64	0.72	0.79
2.36	2.40	2.24	2.86	3.30	4.63	3.93	3.53	4.20	2.30	2.46	2.73
0.45	0.48	0.43	0.54	0.62	0.54	0.70	0.65	0.78	0.43	0.44	0.50
3.00	3.14	2.85	3.52	4.04	3.47	4.63	4.11	5.05	2.78	2.85	3.23
0.67	0.72	0.65	0.74	0.90	0.76	1.01	0.92	1.12	0.63	0.60	0.71
1.91	2.08	1.94	2.28	2.55	2.16	2.87	2.67	3.24	1.88	1.81	2.03
–				2.67	2.67	2.46	2.53	2.46	2.21	2.72	2.10
1.88	2.02	1.86	2.14	2.40	1.99	2.69	2.42	2.98	1.69	1.56	1.83
0.30	0.31	0.28	0.34	0.36	0.30	0.40	0.36	0.45	0.25	0.24	0.28
0.86	0.87	0.86	0.94	0.96	1.03	0.99	1.05	0.76	0.93	0.89	0.99
0.88	0.86	0.88	0.88	0.80	0.85	0.81	0.90	0.56	0.85	0.69	0.76
0.85	0.85	0.85	0.92	0.92	1.02	0.94	1.06	0.62	0.91	0.82	0.93

contrast, clinopyroxene is generally well preserved in all rock-types but is partially replaced by actinolite in the groundmass.

The pillow basalts display aphyric textures with few millimeter-sized olivine and plagioclase phenocrysts. Their groundmass consists of Ti-magnetite and quenched plagioclase and clinopyroxene microlites, which exhibit bow-tie and dendritic textures. Glass is replaced by chlorite. Calcite and/or zeolites filled vesicles may occur.

The Mg-rich basalts occur as massive flows and display aphyric to porphyritic textures. When aphyric, the matrix is composed of clinopyroxene and plagioclase microlites with sometimes, olivine pseudomorph microcrysts. The oxides are the last to crystallize. When the texture is porphyritic, the basalts are composed of olivine and clinopyroxene phenocrysts and microlites of clinopyroxene and plagioclase in the mesostasis. The euhedral habits of the olivine pseudomorphs are always preserved. Differences between samples are expressed by the olivine abundance (6% to 12%) and size (0.5 to 2 mm). Pyroxene is mainly diopside (Wo_{40-45}, En_{47-49}, Fs_{6-7}) and represents the predominant phase (between 50% and 60% in the matrix). It occurs either as isolated phenocrysts or as glomeroporphyritic clots (<5%). Plagioclase forms essentially microlites. The rare pillow-lavas exhibit aphyric or intersertal texture with plagioclase laths and clinopyroxene microcrysts in a silicified matrix.

Ankaramites differ from the Mg-rich basalts by the presence of abundant and large (up to 2 cm-sized) clinopyroxene phenocrysts (5 to 10%). Their fine-grained groundmass includes abundant clinopyroxene, plagioclase and olivine microcrysts. 98G4 differs from the other rocks by the presence of abundant altered plagioclase microlites.

Dolerites exhibit an ophitic texture and are formed of millimeter-sized plagioclase laths cemented by clinopyroxene and late crystallizing oxides. Their groundmass is largely recrystallized into secondary quartz, epidote, and smectite with chlorite and calcite-filled veins.

Picrites are formed of clinopyroxene microphenocrysts with olivine pseudomorphs. Clinopyroxene has a diopside composition (Wo_{44-48}, En_{47-51}, Fs_{5-10}). The matrix is essentially composed of clinopyroxene microcrysts and few needle-shape Fe–Ti oxides. The modal composition of the olivine ranges from 20% to 50%. All the picrites are highly vesicular with quartz, or calcite or smectites-filled large vesicles.

4. Geochemistry

4.1. Analytical methods

All the igneous rocks have experienced variably hydrothermal alteration. Thus, only the samples with well-preserved original igneous mineralogy (i.e., clinopyroxene, olivine, and plagioclase) and devoid of any significant alteration were selected for study. Minerals were separated and then purified by hand picking.

For Sr and Nd isotopic analyses, mineral separates and whole-rocks were leached in a 2 N HCl–0.1 N HF mixture. For Pb isotope determinations, mineral separates and whole rocks were successively leached in hot 2 N HCl for 20 min in an ultrasonic bath, and rinsed with tridistilled water in an ultrasonic bath for 15 min.

Major element analyses were performed by X-ray fluorescence at the Institut de Minéralogie et Pétrographie of the Lausanne University (Switzerland). Trace elements were analyzed by inductively coupled plasma mass spectrometry (ICP-MS) at the University of Grenoble after acid dissolution. Trace elements are spiked with pure Tm using procedures described by Barrat et al. (1996). Standards used for the analyses were JB2, WSE, BIR-1, JR1, and UBN. Major and trace element analyses of host rocks and their mineral separates are presented in Tables 1 and 2.

The $^{143}Nd/^{144}Nd$ and $^{87}Sr/^{86}Sr$ isotopic data were determined on a Finnigan MAT261 multicollector mass spectrometer at the Laboratoire de Géochimie de l'Université Paul Sabatier (Table 3), using the analytical procedures of Lapierre et al. (1997). The chemical separation of lead was carried out following

Notes to Table 1:
Analyses reported on dry basis. LOI added for information.
–: Not analysed.

the procedure modified from Manhès et al. (1978). Total Pb blanks are less than 65 pg for a 100-mg sample. The Pb isotopic ratios were measured on the MC-ICP-MS P54 at the Ecole Nationale Supérieure de Lyon (Table 3). The complete isotopic data set has been corrected for in situ decay assuming an age of 90 Ma, based on the age of the CCOP oceanic plateau rocks.

4.2. Major and trace elements

The degree of alteration of the analyzed rocks is variable. The loss of ignition (LOI, Table 1) varies between 1.3% and 7.1%. This geochemical study is based on the most immobile elements like the rare earth (REE) and high field strength elements (HFSE).

Major and trace element analyses of the samples from each group are reported in Table 1. Ankaramites and basalts exhibit a large range of MgO contents (6.78 to 15 wt.%). Only one sample has a higher content (17.4%). In contrast, the dolerites and isotropic gabbro show a narrow range of MgO contents (5.5 to 8.9 wt.%). The picrites differ from the basalts and ankaramites by significantly higher MgO contents (between 19.9% and 27.3 wt.%). The distinction into two groups is clearly shown in the major element plots (Fig. 4). The dolerites, basalts and ankaramites cluster into one group characterized by the highest contents in Al_2O_3 and SiO_2 (Fig. 4). Among the latter, CaO exhibits the largest range of abundances. This likely expresses alteration processes (i.e., calcite-filling vesicles or cracks). However, the ankaramites have the highest CaO contents (up to 18%) probably related to the abundance of the clinopyroxene phenocrysts. Mafic rocks have also a wide range of trace element concentrations (Ni, Cr and Zr; Fig. 4) at approximatively constant MgO level (6–7%). All the rocks including the picrites have relatively similar FeO concentrations (Fig. 4).

The picrites display a linear trend in all diagrams. They have the highest Cr and Ni contents, which correlate with the highest MgO values. Their incompatible trace elements abundances like Zr and Ta are the lowest of the analyzed rocks. The most MgO-enriched picrite is relatively depleted in SiO_2, TiO_2, Al_2O_3 and CaO. In the Ni and Cr vs. MgO plots (Fig. 4), the mafic rocks and picrites exhibit a good correlation trend whereas the picrites and dolerites represent the less and the most differentiated rocks of this suite, respectively. This reflects the key role of olivine and clinopyroxene in the crystal fractionation of these rocks.

Basalts and dolerites exhibit similar mostly flat primitive-mantle normalized diagrams characterized by positive Sr and negative Th anomalies. The observed positive and negative anomalies of the large ion lithophile elements (LILE, i.e., Ba, Rb, K) probably reflect the alteration and/or low grade metamorphism experienced by these rocks. The isotropic gabbro (99PE25) differs from the dolerites by negative anomalies in Ti and P and lower contents in all the trace elements (Fig. 5).

Compared to the basalts and dolerites, the ankaramites differ by a depletion in Y, and an enrichment in Nb and Ta. The positive or negative Sr anomalies reflect plagioclase accumulation or removal. The picrites exhibit negative anomalies in Th and Sr. Compared to the basalts, dolerites and ankaramites, they have low abundances in incompatible elements like Ta, Nb, Zr and Hf but show Ta and Nb positive anomalies (Fig. 5).

4.3. REE compositions of the igneous rocks and their host minerals

Basalts and dolerites have nearly flat REE patterns (Sun and McDonough, 1989) (Fig. 5) with $(La/Yb)_n$ ratios ranging between 0.73 and 1.06 with the exception of the Guayaquil basalts and the isotropic gabbro. Guayaquil basalts are LREE-depleted ($(La/Yb)_n$ similar to N-MORB) while the isotropic gabbro is slightly LREE enriched ($(La/Yb)_n = 1.23$). Compared to the basalts, the dolerites have a wider range of REE contents and appear to be more fractionated.

Ankaramites exhibit slight (L)REE-enriched patterns (Fig. 5; $1.8 < (La/Yb)_n < 1.3$). Compared to the basalts and dolerites, they differ by a depletion in heavy (H)REE. The positive or negative Sr anomalies reflect plagioclase accumulation or removal. Clinopyroxene separates from four ankaramites (97G4, 98G4, 98G9, 98G12) are depleted in LREE [$0.27 < (La/Yb)_n < 0.69$] and have lower REE contents compared to their host rocks (Fig. 5).

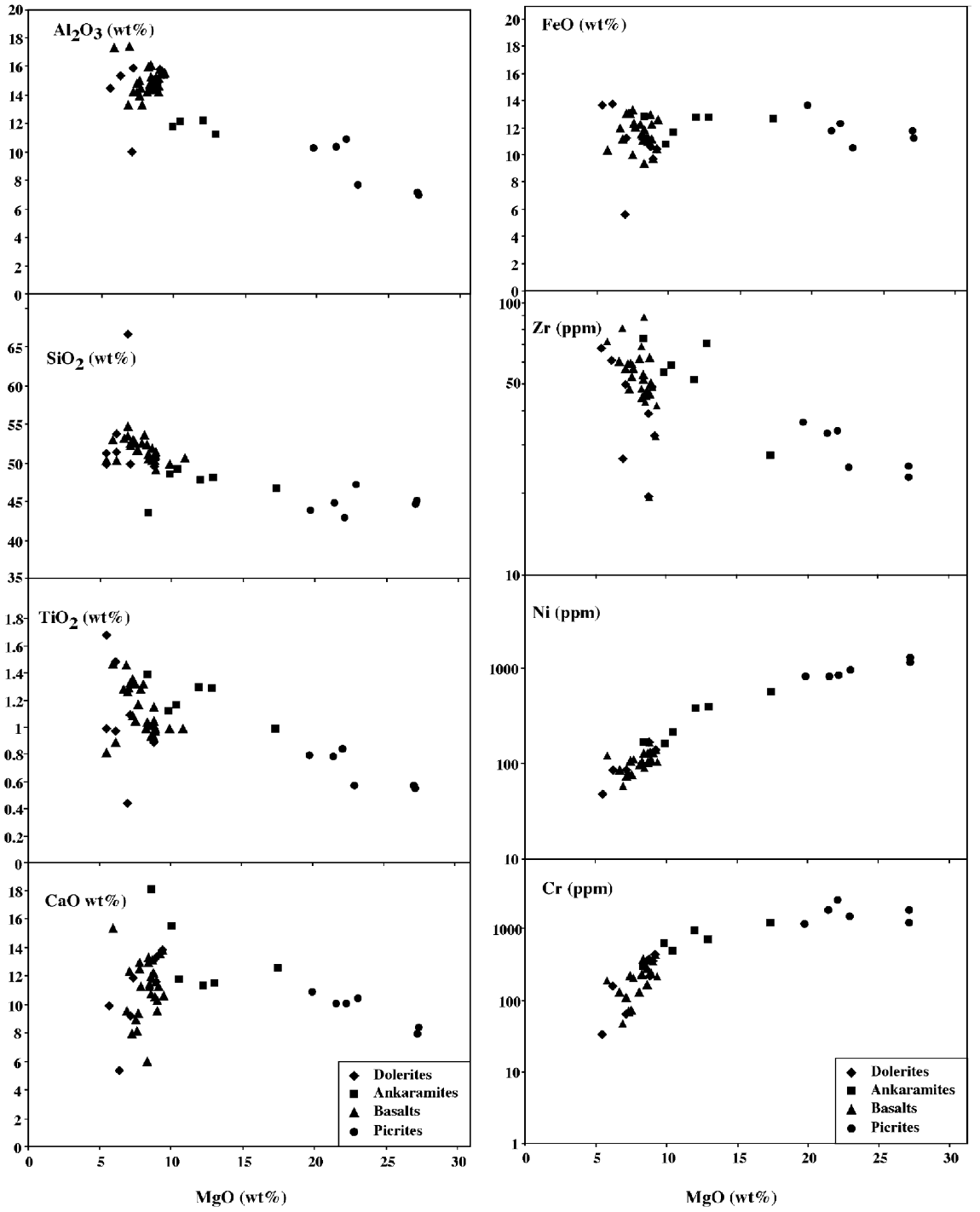

Fig. 4. Al_2O_3 (wt.%), SiO_2 (wt.%), TiO_2 (wt.%), CaO (wt.%), FeO (wt.%), Zr (ppm), Ni (ppm), and Cr (ppm) vs. MgO (wt.%) correlation diagrams of dolerites, ankaramites, basalts and picrites.

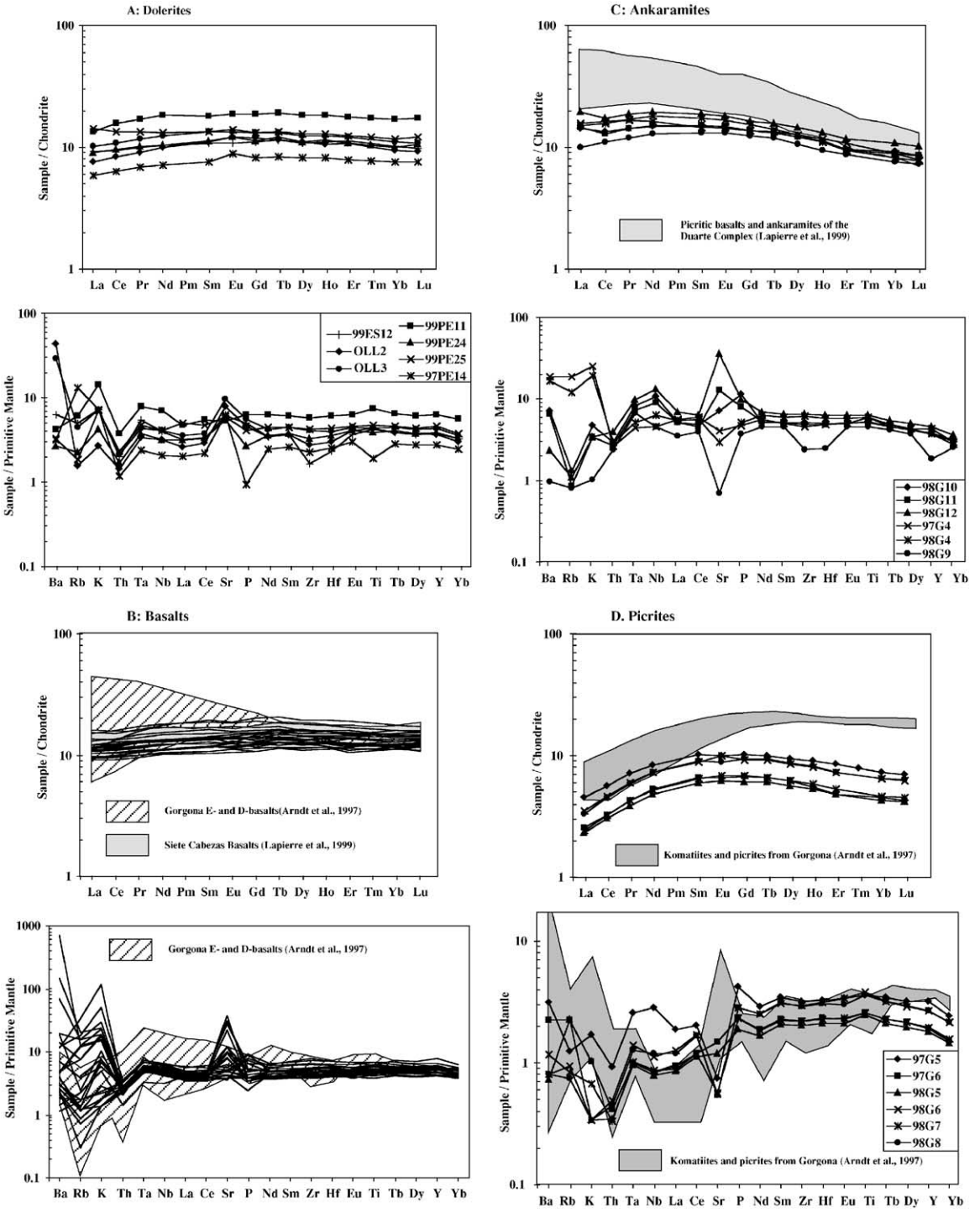

Fig. 5. Chondrite- and primitive mantle-normalized (Sun and McDonough, 1989) rare earth element patterns and multi-element plots for dolerites (A), basalts (B), ankaramites (C) and picrites (D).

The picrites have low REE contents and hamped-shaped patterns, slightly depleted in LREE relative to the HREE (Fig. 5). Clinopyroxene separates from four picrites (97G5, 97G6, 98G5, 98G7) have, like those of the ankaramites, lower REE contents than their host rocks but are more depleted in LREE than those of the ankaramites ($0.25 < (La/Nd)_n < 0.47$, $1.17 < (Sm/Yb)_n < 1.31$, Fig. 6).

4.4. Nd, Sr and Pb isotopic chemistry

The isotopic compositions of Nd, Sr and Pb of the studied rocks and their mineral separates are reported in Tables 2 and 3, respectively.

The basalts have the lowest εNd_i values (+6.1 to +9.2). The clinopyroxene separates of the ankaramites and whole rocks have rather similar and restricted range of εNd_i (+7.0 to +8.2) which are slightly higher than those of the basalts (Tables 2 and 3). The picrites exhibit the highest and largest range of εNd_i values (between +7.7 and +10.2). The clinopyroxene separates from the picrite (98G7) also posses the high εNd_i values (Tables 2 and 3; Fig. 7; +9.8 and +10) which are similar to that of the whole rock.

The ankaramites display a restricted range of $(^{87}Sr/^{86}Sr)_i$ ratios (0.70301 to 0.70348) while the picrites posses lower $(^{87}Sr/^{86}Sr)_i$ (0.70297 to 0.70311) (Table 3). The basalts span a wide range of $(^{87}Sr/^{86}Sr)_i$ (0.70416 to 0.70469) which are the highest of the studied rocks and suggest that the basalts were more intensely affected by alteration than the picrites and ankaramites (Fig. 7). In Fig. 7, the ankaramites plot in the Galápagos field and near that of the depleted and enriched basalts from Gorgona. The picrites fall in the Gorgona komatiites field.

Lead initial isotopic compositions of the whole rocks are reported in Table 3 and fall into three groups in the Pb/Pb correlation diagrams (Fig. 8). The first group, constituted by the most radiogenic Pb samples, consists of four of the ankaramites and one dolerite ($19.59 < (^{206}Pb/^{204}Pb)_i < 19.71$). This group plots in the field of the picrites and Mg-rich basalts from southwestern Colombia (Kerr et al., in press) and the Duarte Mg-rich basalts and ankaramites from Dominican Republic (Lapierre et al., 2000). The second group, composed of four picrites and two basalts is the least radiogenic in Pb ($18.29 < (^{206}Pb/^{204}Pb)_i < 18.40$). The third group, which is composed of all the remaining dolerites and basalts (with the exception of 99PE19), one picrite and two ankaramites, is characterized by Pb isotopic compositions ($18.56 < (^{206}Pb/^{204}Pb)_i < 19.01$) intermediate between the groups 1 and 2.

Most of the Ecuadorian mafic to ultramafic lavas display a linear but discontinuous trend in diagrams

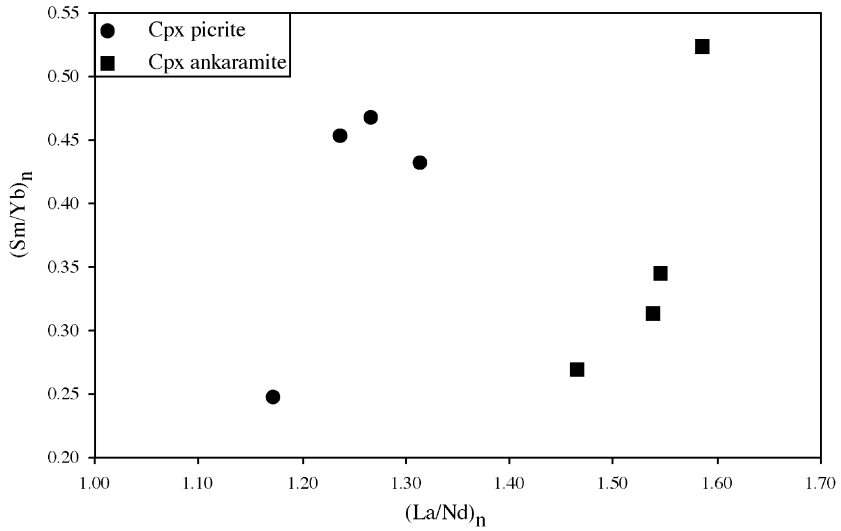

Fig. 6. $(Sm/Yb)_n$ vs. $(La/Nd)_n$ correlation diagram for clinopyroxene of picrites and ankaramites from Guaranda cross-section.

Table 2
Major (wt.%), trace element (ppm) and isotopic analyses for the Guaranda mineral separates

Sample	97G4 Cpx	98G4 Cpx	98G4-2 Cpx	98G9 Cpx	98G12 Cpx	98G12 Cpx	97G5 Cpx	97G6 Cpx	98G5 Cpx	98G7 Cpx	98G7 Cpx
Host rock	Ankaramite	Ankaramite	Ankaramite	Ankaramite	Ankaramite	Ankaramite	Picrite	Picrite	Picrite	Picrite	Picrite
Fraction (μm)	100/125	80/100	100/125	125/160	80/100	100/125	100/125	100/125	100/125	80/100	100/125
Ba	18.85	29.86		2.38	2.29		–	–	5.20	6.26	
Rb	3.12	1.59		0.07	0.11		0.27	0.57	0.54	0.40	
Sr	13.58	24.22		11.78	32.45		12.59	22.85	21.17	15.76	
Ta	0.00	0.07		0.01	0.03		0.01	0.03	0.06	0.05	
Th	–	0.08		0.01	0.02		0.00	0.02	0.04	0.04	
Zr	9.55	35.55		10.94	17.79		10.54	25.01	29.35	29.18	
Nb	0.07	1.09		0.09	0.57		0.09	0.47	0.85	0.69	
Y	7.77	–		–	–		8.55	10.31	–	–	
Hf	0.44	1.35		0.55	0.92		0.49	0.76	1.01	0.99	
Co	44.11	–		–	–		38.58	82.32	–	–	
U	–	0.04		0.01	0.02		–	–	0.02	0.02	
Zn	18.94	–		–	–		16.62	34.05	–	–	
La	0.24	1.12		0.31	0.49		0.17	0.54	0.68	0.74	
Ce	0.91	3.53		1.20	1.84		0.66	1.89	2.24	2.58	
Pr	0.22	0.66		0.26	0.40		0.18	0.37	0.43	0.51	
Nd	1.70	4.15		1.91	2.74		1.33	2.30	2.81	3.33	
Sm	0.81	1.62		0.91	1.20		0.71	0.99	1.18	1.33	
Eu	0.33	0.65		0.38	0.48		0.29	0.42	0.50	0.56	
Gd	1.22	2.31		1.46	1.87		1.16	1.39	1.76	1.98	
Tb	0.20	0.39		0.25	0.32		0.20	0.25	0.31	0.34	
Dy	1.46	2.59		1.70	2.18		1.48	1.71	2.12	2.36	
Ho	0.28	0.51		0.32	0.42		0.30	0.36	0.43	0.47	
Er	0.72	1.32		0.82	1.05		0.78	1.00	1.16	1.26	
Tm	2.71	0.18		0.11	0.14		2.69	2.73	0.16	0.17	
Yb	0.60	1.09		0.63	0.83		0.64	0.86	0.99	1.09	
Lu	0.08	0.16		0.10	0.13		0.10	0.13	0.16	0.17	
$(Ce/Yb)_n$	0.40	0.84		0.49	0.57		0.27	0.57	0.58	0.61	
$(La/Sm)_n$	0.18	0.44		0.21	0.25		0.15	0.34	0.36	0.35	
$(La/Yb)_n$	0.27	0.69		0.33	0.39		0.18	0.42	0.46	0.46	
$^{143}Nd/^{144}Nd$		0.513052	0.513054	0.513086	0.513011	0.512991				0.513171	0.513179
2σ		± 8	± 22	± 21	± 25	± 16				± 16	± 12
$^{147}Sm/^{144}Nd$		0.236020	0.236020	0.288067	0.264794	0.264793				0.241491	0.241492
$(^{143}Nd/^{144}Nd)_i$		0.512913	0.512915	0.512916	0.512855	0.512835				0.513029	0.513037
εNd_i		+7.63	+7.67	+7.69	+6.5	+6.11				+9.89	+10.04

–: Not analysed.

where εNd is plotted against MgO, $(La/Yb)_n$ and $(^{206}Pb/^{204}Pb)_i$ (Fig. 9). This suggests that (i) the basalts, dolerites, and one picrite could derive from the mixing of both depleted and enriched sources; (ii) the variations of the MgO content and $(La/Yb)_n$ ratios within each rock group are largely dependent on the extent of partial melting. The Pb isotopic compositions of the depleted and enriched end-members sources could be similar to those of the most depleted picrite (97G6) and enriched ankaramite (98G12; Table 3).

4.5. Calculated melts in equilibrium with the clinopyroxenes

Eight clinopyroxenes were separated from ankaramitic and picritic host rocks. The trace element compositions of the clinopyroxene separates (including the REE) are reported in Table 2.

The REE compositions of the parent melts in equilibrium with the clinopyroxene separates from picrites and ankaramites were calculated using the partition coefficients of Ulmer (1989) and Shimizu et

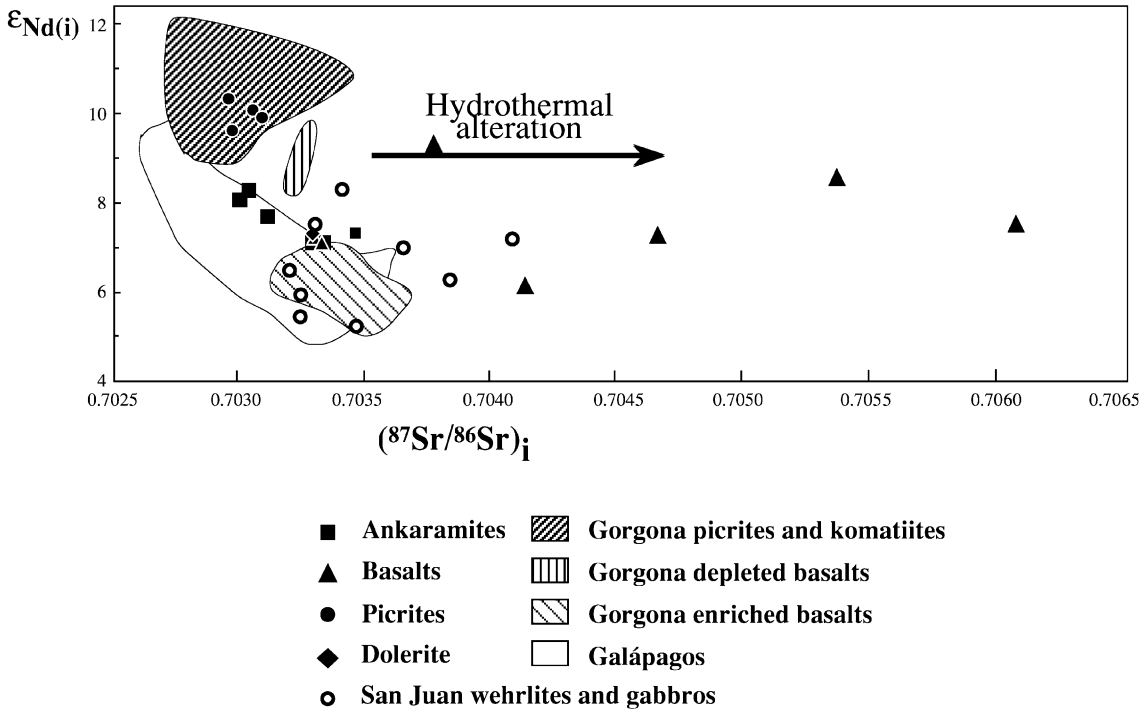

Fig. 7. εNd_i–$(^{87}Sr/^{86}Sr)_i$ plots for ankaramites, picrites and basalts from the Guaranda cross-section, and from San Juan unit (Mamberti et al., submitted for publication) and Piñon Formation (Reynaud et al., 1999; Lapierre et al., 2000).

al. (1982) for the picrites, and of Hart and Dunn (1993) for the basalts. It was difficult to choose the partition coefficient for the ankaramites because such coefficients for ankaramitic melts are not available in the literature. So, for the ankaramites, we used the basaltic partition coefficients.

Picritic (Fig. 10A) and ankaramitic (Fig. 10B) melts in equilibrium with the clinopyroxene separates from picrites and ankaramites share in common with the host rocks similar LREE-depleted patterns (except for 97G5). However, these theoretical melts differ from the lavas by a slightly LREE-enrichment ($1.02 < (La/Yb)_n < 1.11$) and higher REE abundances. This is due to the presence of olivine that leads to a dilution of the REE contents in the host rock. This reflects also the key role of clinopyroxenes in controlling REE abundances of the Ecuadorian picrites and ankaramites.

Two rocks are exceptions and illustrate the complexity of using partition coefficients. The REE composition of the calculated melts using picrite 97G5 and ankaramite 98G4 clinopyroxene separates match only with the host rocks on the basis of the partition coefficients for basalt and picrite, respectively. This is the opposite of what we should expect. This is probably linked to differences in temperature and/or pressure for condition of crystallization of these two rocks (97G5, 98G4), compared to the other picrites and ankaramites.

5. Discussion

5.1. Summary of the petrological, mineralogical and geochemical data

Basalts, dolerites and shallow level gabbros represent the most widespread oceanic rock types of southwestern Ecuador (Pinón Formation, Manta area, Pallatanga unit). They are characterized by homogeneous petrological and geochemical features, i.e., low MgO contents, mostly flat REE patterns, rather restricted range of εNd_i and Pb isotopic compositions.

Table 3
Nd, Sr and Pb isotopic compositions for the Guaranda, Galán, Pedernales and Esmeraldas rocks and mineral separates

Sample	Name	$(^{206}Pb/^{204}Pb)_i$	$(^{207}Pb/^{204}Pb)_i$	$(^{208}Pb/^{204}Pb)_i$	$(^{87}Sr/^{86}Sr)_m$	2s	$^{87}Rb/^{86}Sr$	$(^{87}Sr/^{86}Sr)_t$	ε $(Sr)_i$	Sm	Nd	Sm/Nd	$(^{143}Nd/^{144}Nd)_m$	2s	$^{147}Sm/^{144}Nd$	$(^{143}Nd/^{144}Nd)_i$	ε $(Nd)_i$
97G2	Dolerite	19.24	15.55	38.79						2.7	7.9	0.34					
99PE11	Gabbro									2.9	8.9	0.32					
97PE14	Dolerite				0.705110	± 6	0.18247	0.704877	6.85	1.2	3.4	0.35	0.513017	± 12	0.211720	0.512892	+7.22
99PE24	Dolerite									1.7	5	0.35					
99PE25	Dolerite	18.80	15.56	38.40	0.703632	± 6	0.02657	0.703598	− 11	2.1	6.3	0.33					
99ES12	Dolerite	18.62	15.56	38.26						1.69	4.94	0.33					+7.82
97G4	Ankaramite	18.81	15.52	38.46	0.703568	± 9	0.39982	0.703057	− 19	2.2	7.7	0.29	0.513046	± 9	0.176118	0.512942	+8.20
98G4	Ankaramite	18.58	15.53	38.39	0.703476	± 9	0.36080	0.703015	− 20	2.7	8.5	0.31	0.513043	± 5	0.189691	0.512931	+7.98
98G9	Ankaramite	19.59	15.59	39.12	0.703261	± 12	0.10152	0.703131	− 18	2	6.1	0.33	0.513030	± 7	0.199561	0.512913	+7.62
98G10	Ankaramite	19.71	15.61	39.19	0.703327	± 8	0.01539	0.703307	− 15	2.3	7	0.33	0.512999	± 7	0.197957	0.512882	+7.03
98G11	Ankaramite	19.67	15.61	39.19	0.703487	± 18	0.00581	0.703480	− 13	2.3	7.1	0.32	0.513009	± 5	0.195408	0.512894	+7.25
98G12	Ankaramite	19.65	15.60	39.17	0.703352	± 8	0.00260	0.703349	− 15	2.9	9.2	0.31	0.512994	± 5	0.190161	0.512882	+7.02
97PE5	Pillow				0.705007	± 6	0.04503	0.704949	7.88	2	5.9	0.34					
97PE6	Pillow				0.703385	± 7	0.02925	0.703348	− 15	1.9	5.8	0.33	0.513001	± 9	0.198330	0.512884	+7.06
97PE13	Basalt				0.706341	± 8	0.16745	0.706127	24.6	2.1	6.5	0.33	0.513023	± 7	0.200417	0.512905	+7.50
97G11	Basalt									1.9	5.4	0.34	0.512996	± 7	0.207870	0.512874	+6.86
97G12	Basalt									1.7	5	0.34	0.512985	± 9	0.203150	0.512865	+6.77
97Ma16	Basalt	18.77	15.59	38.44						1.1	2.92	0.38	0.513043	± 10	0.205905	0.512877	+7.81
98P3	Basalt				0.704760	± 15	0.05336	0.704692	19.2	2.4	7	0.33	0.51301	± 12	0.202396	0.512891	+7.19
98P7	Basalt	18.98	15.58	38.54						1.9	5.4	0.35	0.513059	± 6	0.208860	0.512936	+8.07
98P8	Basalt	18.82	15.59	38.40						1.6	4.9	0.34	0.513060	± 7	0.203120	0.512940	+8.16
98P10	Pillow				0.704169	± 10	0.00521	0.704162	− 3.3	2.2	6.5	0.34	0.512954	± 9	0.205154	0.512833	+6.07
99PE15	Basalt									2.1	6.2	0.33					
99PE16	Hyaloclastite	19.01	15.56	38.63	0.703940	± 6	0.11203	0.703797	− 8.5	1.7	5	0.34	0.513115	± 34	0.203244	0.512995	+9.23
99PE19	Basalt	18.34	15.60	38.08	0.706320	± 8	0.04265	0.706265	26.6	2.2	6.4	0.34					
99PE20	Basalt	18.86	15.55	38.56	0.705482	± 7	0.05549	0.705411	14.4	2.2	6.5	0.33					
99PE21	Glass	18.66	15.59	38.39	0.706138	± 7	0.05446	0.703315	− 15	1.8	5.3	0.34	0.513012	± 7	0.207950	0.512890	+7.17
99PE22	Pillow	18.94	15.51	38.51	0.705430	± 6	0.01824	0.705407	14.4	1.8	5.4	0.34	0.512074	± 7	0.204700	0.512954	+8.48
99ES1	Hyaloclastite	18.27	15.59	37.98													
99ES5	Hyaloclastite	18.56	15.57	38.32													
99Gy1	Basalt	18.34	15.51	37.84						3.07	8.41	0.37	0.513061	± 9	0.224566	0.512880	+7.80
00LL2	Basalt	18.31	15.56	38.01						1.71	4.81	0.36	0.513013	± 6	0.218954	0.512837	+7.00
00LL3	Basalt									2.08	5.98	0.35	0.513005	± 13	0.214044	0.152833	+6.91
97G5	Picrite	18.31	15.46	38.05						0.9	3.2	0.29	0.513021	± 10	0.173019	0.512919	+7.75
97G6	Picrite				0.703133	± 12	0.12656	0.702971	− 20	0.7	2.1	0.32	0.513160	± 10	0.191713	0.513047	+10.24
98G5	Picrite	18.71	15.55	38.64	0.703201	± 13	0.16646	0.702988	− 20	0.9	2.3	0.40	0.513155	± 15	0.243960	0.513011	+9.54
98G6	Picrite	18.31	15.48	38.11	0.703257	± 13	0.14851	0.703067	− 19	1.4	3.4	0.39	0.513174	± 9	0.238362	0.513034	+9.98
98G7	Picrite	18.40	15.49	38.10	0.703274	± 13	0.12916	0.703109	− 18	1	2.5	0.40	0.513169	± 22	0.241490	0.513027	+9.85
98G8	Picrite	18.29	15.49	38.06						1.4	3.4	0.40	0.513178	± 7	0.244433	0.513034	+9.99

(m): Ratios measured; (i): initial recalculated ratios (90 Ma) based on the U, Th and Pb contents determined by ICP-MS (refer to Table 1).

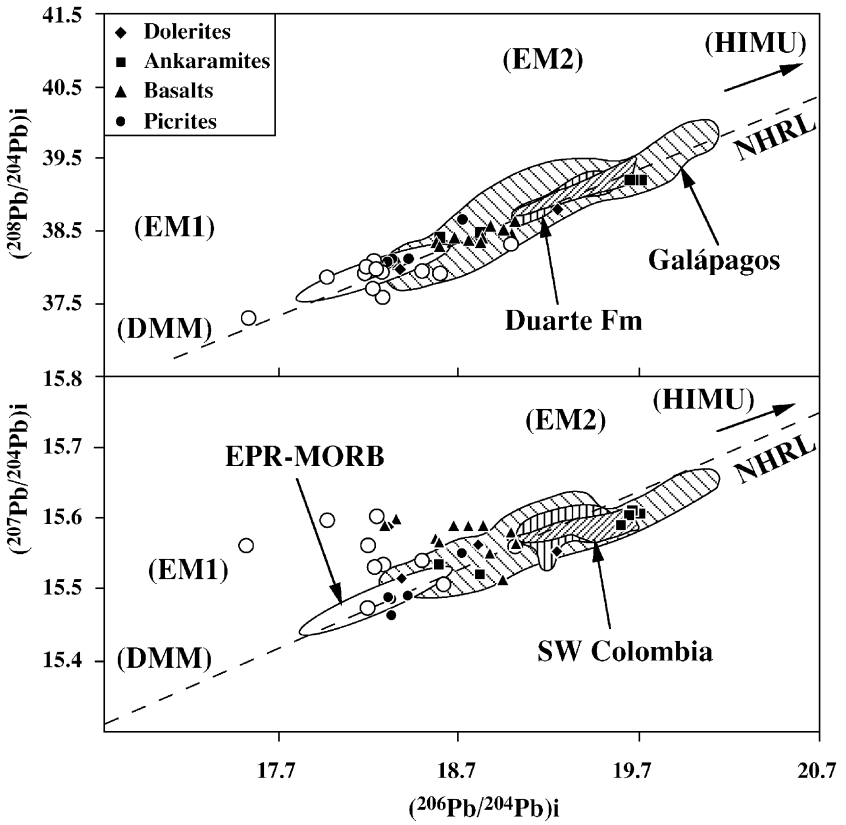

Fig. 8. $(^{208}Pb/^{204}Pb)_i$ vs. $(^{206}Pb/^{204}Pb)_i$ and $(^{207}Pb/^{204}Pb)_i$ vs. $(^{206}Pb/^{204}Pb)_i$ correlation diagrams for dolerites, ankaramites, basalts and picrites. The Pb isotopic ratios from the Early Cretaceous rocks are reported after Lapierre et al. (2000) and Mamberti et al. (submitted for publication). The "Northern Hemisphere Reference Line" (NHRL) and the field from some mantle reservoirs are reported after Zindler and Hart (1986). East Pacific Rise (EPR) MORB and Mid Atlantic Ridge (MAR) MORB data and Galápagos Islands field are from White et al. (1987). The Duarte field is reported after Lapierre et al. (1997). The SW Colombia field is reported after Kerr et al. (in press).

In contrast, picrites are solely exposed near Pedernales and in the western part of the Pallatanga unit. Their Nd and Pb isotopic compositions are similar to those of the most depleted basalts. Finally, the ankaramites and Mg-rich basalts have been solely observed in the Pallatanga unit (Guaranda, Pallatanga, and Galán sections). Relative to the basaltic and picritic melts, they are the most LREE-enriched and derive from the most enriched mantle source.

5.2. Comparison with the nearby Early Cretaceous and Late Cretaceous oceanic plateau sequences

Two crustal fragments of oceanic plateau affinity are exposed in the Western Cordillera of Ecuador and differ in terms of lithologies of their igneous components. They likely represent remnants of two distinct oceanic plateaus or two magmatic events of the same oceanic plateau. The Early Cretaceous crustal fragment consists of cumulate ultramafic and mafic rocks (San Juan sequence) while basalts, dolerites, shallow level isotropic gabbro, ankaramites of the Pallatanga unit belong to the Late Cretaceous event (90–86 Ma) of the Caribbean–Colombian Oceanic Plateau (Boland et al., 2000). Because of the lack of age, it is not yet possible to determine if the basalts exposed near Quillan, Merced–Multitud and Ibarra (Fig. 2) belong to the Early Cretaceous or Late Cretaceous oceanic plateau.

On the basis of the ages of the associated arc-rocks, and in spite of their petrological and geochemical similarities, it is likely that all the mafic rocks of

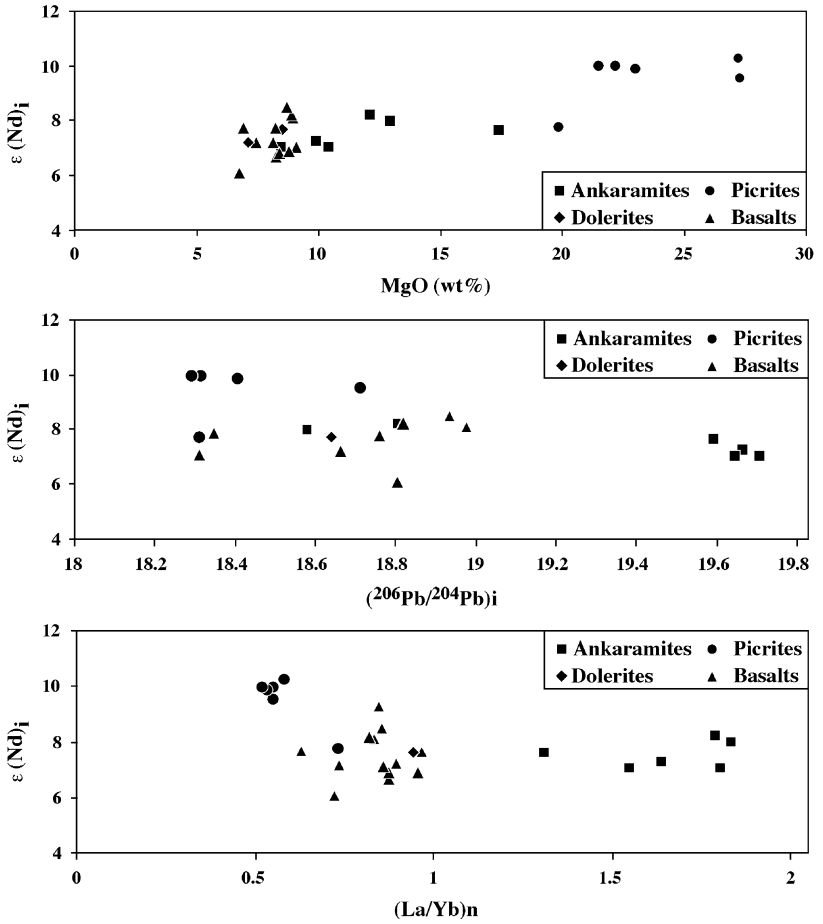

Fig. 9. εNd vs. MgO (wt.%), $(^{206}Pb/^{204}Pb)_i$, and $(La/Yb)_n$ correlation diagrams for ankaramites, basalts and picrites from the Guaranda and Pedernales sequences.

oceanic affinity exposed in Coastal Ecuador do not belong to the same oceanic plateau. The basalts and dolerites exposed in the south (Pinón Formation of the Santa Elena and Guayaquil areas) are pre-Late Cretaceous in age (pre-90 Ma) and could belong to the Early Cretaceous oceanic plateau. The basalts and dolerites outcropping near Manta are most probably younger (85 Ma) and could be related to the Upper Cretaceous (92–86 Ma) lavas of the CCOP. We propose that the igneous rocks of the Manta area belong to the same unit as those of Pedernales, Quinindé and Esmeraldas areas, which will be collectively referred to as the Pedernales unit.

The Pallatanga and Pedernales units appear to be petrologically and geochemically similar to the Upper Cretaceous (92–86 Ma) lavas of the CCOP. These volcanic rocks can be subdivided into two main groups. Group 1 consists of highly depleted komatiites and picrites (Gorgona, Colombia; Fig. 5) characterized by high εNd_i and very low Pb ratios. Group 2 encompasses all the other lavas exposed in the Caribbean (Colombia, Costa Rica, Hispaniola, Curaç ao), i.e., picrites, Mg-rich basalts, ankaramites, and basalts. This second group is characterized by flat to LREE-enriched patterns, εNd_i ranging between +6 and +9.5 (Fig. 7) and Pb isotopic signature consistent with the field defined by the recent Galápagos Islands (Fig. 8), suggesting the contribution of a HIMU component.

The picrites of the Pallatanga unit share with the CCOP Group 1 similar Nd and Pb isotopic composi-

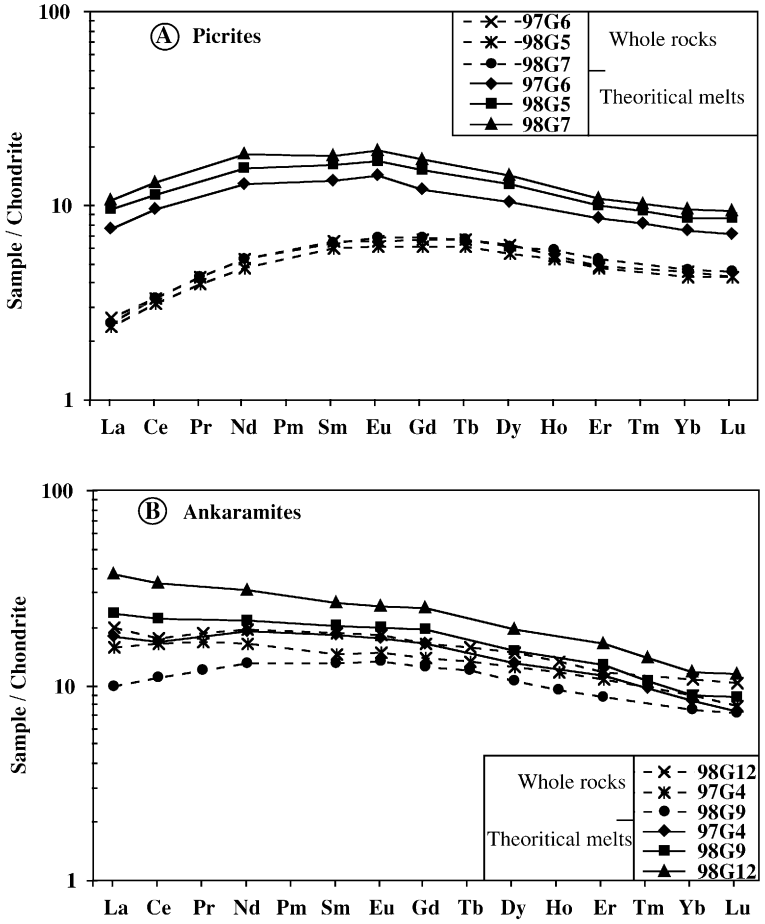

Fig. 10. Chondrite-normalized REE patterns of calculated melts from the cpx of Guaranda picrites (A) and ankaramites (B). The melts are calculated using partition coefficients for picrite and ankaramite (Shimizu et al., 1982; Ulmer, 1989; Hart and Dunn, 1993).

tions (Figs. 7 and 8) but differ from the Gorgona picrites in that they are less depleted in LREE, have lower REE abundances, especially in HREE, and are enriched in Nb and Ta (Fig. 5). The ankaramites, Mg-rich basalts, dolerites and basalts of the Guaranda and Pedernales units exhibit the same trace element patterns and Sr, Nd and Pb isotopic geochemistry as the CCOP Group 2 rocks (Figs. 7 and 8).

One may wonder whether the two distinct oceanic plateau successions of Ecuador may represent two distinct basaltic pulses within the same plateau, as described for the Ontong Java Plateau (OJP) (Neal et al., 1997). Therefore, the Early Cretaceous and Late Cretaceous oceanic plateau successions of Ecuador represent remnants of either two distinct oceanic plateaus or two magmatic events of the same plateau.

5.3. Spatial and temporal relationships between picrites, ankaramites, dolerites and basalts

Field relationships in the Guaranda section allow us to specify that the picrites are stratigraphically overlain by the ankaramites, and that the time span between picrite and ankaramite eruptions was very short. We have no evidence for the stratigraphic relations between the basalts and the more-mafic lavas. The pillow basalts and dolerites are either the uppermost levels of the volcanic pile or the lateral

variations of the ankaramites. The pillow matrix of the Pedernales basalts consists of siliceous pelagic sediments suggesting that these pillowed flows represent the shallower levels of the oceanic plateau crust. The most likely stratigraphic succession for the Ecuadorian complete sequence would be picrites overlain by ankaramites, which are in turn overlain by the pillow basalts and dolerites. This is in agreement with the hypothetical cross-section through the Caribbean oceanic plateau proposed by Kerr et al. (1998).

Trace-element signatures of lavas from the Pallatanga and Pedernales units vary widely from almost enriched LREE patterns in ankaramites to extremely depleted patterns in picrites. Basalts and dolerites exhibit much more homogeneous geochemical features which are those of most oceanic plateaus (flat REE patterns). Trace-element variations within each group of rocks are linked to differences in the extent of partial melting. These contrasting features are also present in the isotopic geochemistry of these rocks. The picrites derived from an extremely depleted source, with initial εNd_i ranging from +10.2 to +7.7 and low Pb isotopic ratios. The source of the ankaramites is less depleted with initial εNd_i ranging from +8.2 to +7, and highly radiogenic Pb isotopic compositions suggesting a HIMU component contribution. The basalts and dolerites have the most homogeneous source with initial εNd_i ranging from +9.2 to +6.1. Their Pb isotopic compositions are intermediate between those of the depleted picrites and enriched ankaramites.

5.4. Multi-stage model for the emplacement of the Ecuadorian picrites, ankaramites and basalts

Field relationships of the picrites, ankaramites and basalts indicate the presence of two types of occurrences: (1) the Guaranda type where picrites are conformably overlain by ankaramites and associated with basalts, (2) and the Pedernales type characterized by the presence of hyaloclastites formed of picritic and basaltic fragments. This indicates that picritic melts are emplaced more or less simultaneously with ankaramitic or basaltic magmas. This is in contradiction with the structure of plume heads where the high temperature material producing picritic or komatiitic magmas is located in the plume axis while the bulk of the plume head will yield low temperatures melts such as basalts (Campbell and Griffiths, 1993).

In order to explain the Guaranda type, we have to suppose that two different crustal plumbing systems occurred simultaneously. The picritic melts ascended rapidly to the surface while the ankaramites and MgO-rich basalts were trapped in magma chambers where they began to differentiate. The emplacement of the picrites shortly followed by the ankaramites was very quick because no magma mixing is observed between the two rock types and the petrological and geochemical features of the depleted picrites and enriched ankaramites are preserved.

The Pedernales type where picritic and basaltic fragments are present within the same hyaloclastite bed suggests that picrites and basalts are coming from the same magma chamber. Such type of occurrence can probably be explained by the sudden replenishment of a mafic magma chamber by picritic melts. The injection of very hot magma in the magma chamber will lead to a convective overturn of the already differentiated basaltic magma and the simultaneous eruption of the picritic and basaltic melts (Révillon et al., 2000b). The presence of quenched olivine in the picritic fragments and the lack of degassing vesicles in the picrite and basalt indicate that this hyaloclastite was formed under shallow water level and that picritic and basaltic magmas ascended quickly to the surface.

The origin and emplacement of the basalts, dolerites and gabbroic stocks are probably very different from that of the picrites and ankaramites. These rocks are the last to be emplaced. Their trace element and isotopic compositions are very homogeneous and do not differ in composition from other oceanic plateau basalts. Thus, they are not representative of an individual plume source components. This change with time in the chemistry of the oceanic plateau lavas from depleted ultramafic melts to very homogeneous basalts through enriched ankaramites indicates that (i) the magmatic system above the plume evolved and (ii) the successive batches of magma mixed and fractionated in deep or intermediate level magma chambers, to generate the later basalts and dolerites (Kerr et al., 1998).

The Ecuadorian picrites likely derived from the hot part of the plume and ascended directly to the surface without being trapped in intermediate magma cham-

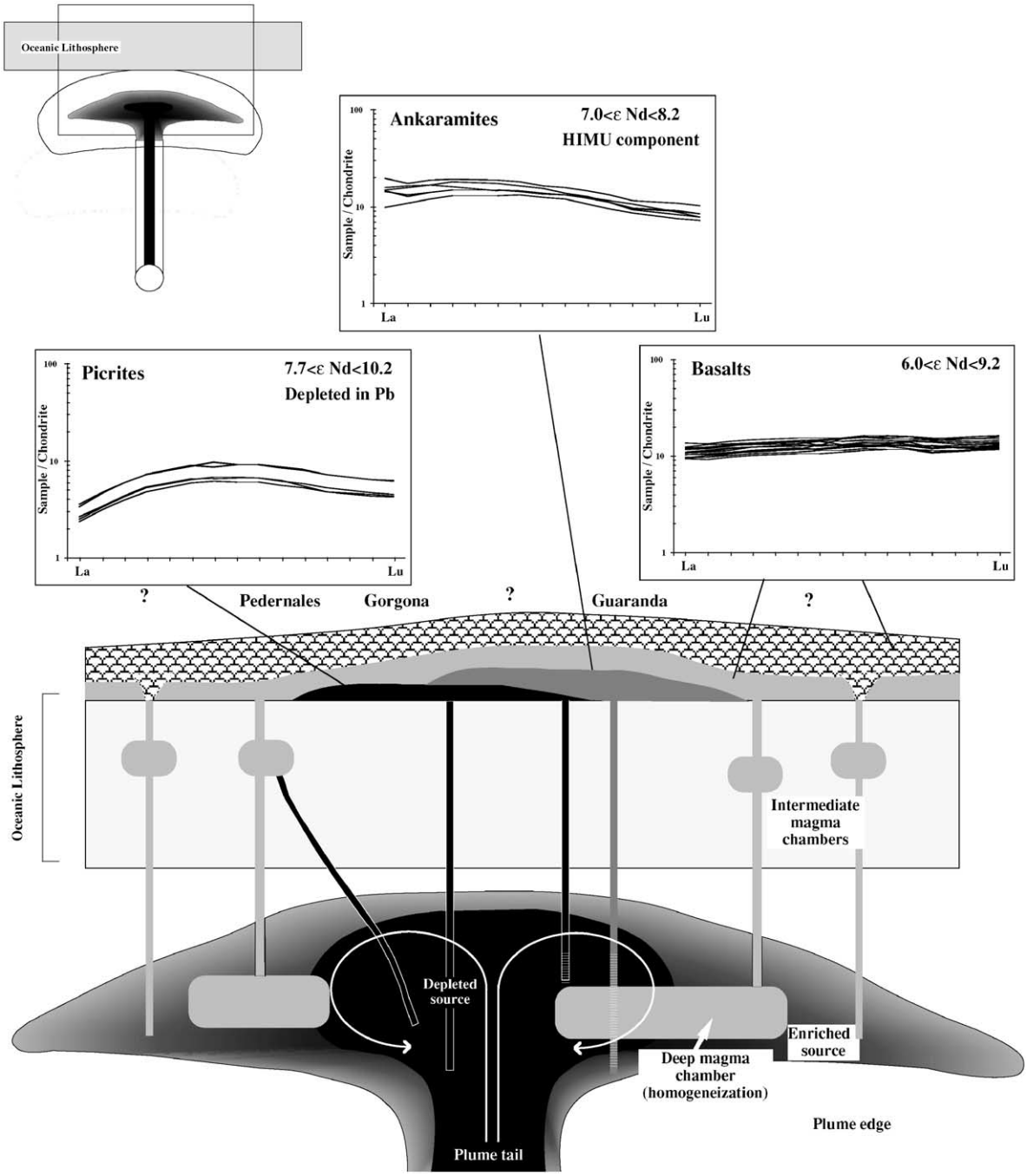

Fig. 11. Spatial and temporal relationships between the picritic, ankaramitic and basaltic magmas. Picrites are extracted from a depleted mantle source located in the very hot plume tail and ascended directly to the surface. Some of these liquids were trapped in magma chambers where they mixed with more fractionated melts. Ankaramites and Mg-rich basalts are extracted from an enriched source located in the plume edges and ascended to the surface or were trapped in intermediate magma chambers where they differentiated or mixed with more evolved melts. Finally, basalts and dolerites derived from mixed and fractionated magmas trapped in deep or intermediate magma chambers.

bers. These ultramafic melts derived from an extremely depleted source with high extents of partial melting (cf. 20% to 25%; Révillon et al., 2000b). The ankaramitic melts were more probably extracted from an enriched source of the plume. The rather high MgO contents ($17.4 < MgO\% < 8.5$) of these rocks suggests that most of them ascended to the surface. The trace element variations of the ankaramites (especially the LREE-enrichment) are likely linked to the differences in the amount of partial melting, which are significantly lower than in the picrites. The depleted and enriched sources of the plume likely derive from recycled oceanic lithosphere (ultramafic and mafic cumulates and hydrothermally altered basalts; Kerr et al., 1998).

In view of the close spatial and temporal relationships between the picritic, ankaramitic and basaltic magmas, it appears obvious that the source of the Ecuadorian magmas was originally heterogeneous on a small scale. As previously proposed by Révillon et al. (2000b), and shown in Fig. 11, a multi-stage model can potentially explain the stratigraphic succession from picrites to basalts through ankaramites, and the contrasting geochemical and isotopic features of these plume-related rocks.

Komatiites, picrites and ankaramites occur only in the CCOP and are as yet unknown in large Mesozoic oceanic plateaus like the Ontong Java where only geochemically homogeneous basalts have been described (Mahoney et al., 1993; Neal et al., 1997). This indicates that in the Caribbean–Colombian province, the deeper sections of the plateau have been uplifted (Kerr et al., 1998) and exposed, thanks to subsequent erosion, allowing direct sampling and study of the depleted and enriched plume components.

6. Conclusions

Crustal fragments of oceanic plateau affinity exposed in Ecuador likely belong to two distinct oceanic plateaus which differ mainly in their rock lithologies and Pb isotopic compositions.

The oldest plateau sequence, of Early Cretaceous age (≈ 123 Ma), consists of ultramafic and mafic cumulate rocks. All the igneous rocks have low Pb isotopic ratios and display a rather large range of εNd_i (from $+10$ up to $+4$) but most values cluster at $+7$. This suggests that the Early Cretaceous oceanic plateau rocks derived from a rather depleted mantle source. The basalts and dolerites of the Piñon Formation exposed in southwestern Coastal Ecuador could represent fragments of the Early Cretaceous oceanic plateau.

The youngest plateau sequence (≈ 90 Ma) is composed of picrites, ankaramites, Mg-rich basalts, basalts, dolerites and shallow level gabbros. The LREE-depleted picrites derived from a depleted source, characterized by high εNd ratios and very low Pb isotopic ratios. In contrast, the LREE-enriched ankaramites and Mg-rich basalts differ from the picrites by lower εNd_i and higher radiogenic Pb isotopic compositions, and are very similar to the Galápagos HIMU component. They exhibit homogeneous εNd_i ($+6$ to $+9$), and Pb ratios intermediate between those of the picrites and ankaramites. The ankaramites and Mg-rich basalts differ from the Early Cretaceous cumulate rocks by higher $^{206}Pb/^{204}Pb$ ratios. The Ecuadorian picrites, ankaramites and Mg-rich basalts bear striking similarities with those of the Late Cretaceous (92–86 Ma) Caribbean–Colombian Oceanic Plateau, of which this sequence may represent an accreted fragment. Fragments of this plateau have been identified in the Western Cordillera of Central Ecuador (Pallatanga Unit) and in the northern part of coastal Ecuador (Pedernales unit).

The field observations and geochemical data on the Late Cretaceous plume-related rocks support: (1) plume heterogeneity leading to the spatial association of picrites with ankaramites and basalts and (2) a multi-stage model for the emplacement of the Late Cretaceous plume-related rocks. Moreover, the temporal evolution from depleted picrites to homogeneous mildly enriched basalts through highly enriched ankaramites indicates that the heterogeneity and specific isotopic features of the mantle plume source decrease with time. In contrast with the picrites and ankaramites, which ascended directly to the surface, the basaltic melts were stored in deep or intermediate magma chambers where they mixed and fractionated.

Acknowledgements

This research has been supported by grants from INSU-CNRS (Intérieur de la Terre) and FNRS No. 20-50812.97 to M. Polvé and J. Hernandez, respectively. Thanks to F. Sénebier who did all the mineral

separates. We would like to thank P. Telouk and the Service Commun National du MC-ICPMS de l'Ecole Normale de Lyon, as well as P. Brunet (UMR-5563), who carried out all the Sr–Nd TIMS analyses. A.C. Kerr and C.W. Sinton are acknowledged for their constructive and thorough reviews.

References

Aitken, B.G., Echeverria, L.M., 1984. Petrology and geochemistry of komatiites from Gorgona island Colombia. Contrib. Mineral. Petrol. 86, 94–105.

Arculus, R.J., Lapierre, H., Jaillard, E., 1999. A geochemical window into subduction–accretion processes: the Raspas Metamorphic Complex, Ecuador. Geology 27, 547–550.

Arndt, N.T., Kerr, A.C., Tarney, J., 1997. Dynamic melting in plume heads: the formation of Gorgona komatiites and basalts. Earth Planet. Sci. Lett. 146, 289–301.

Aspden, J.A., McCourt, W.J., 1986. Mesozoic oceanic terrane in the Central Andes of Colombia. Geology 14, 415–418.

Barrat, J.-A., Keller, F., Amossé, J., Taylor, R.N., Nesbitt, R.W., Hirata, T., 1996. Determination of rare earth elements in sixteen silicate reference samples by ICP-MS using a Tm addition and an ion-exchange chromatography procedure. Geostand. Newsl. 20, 133–139.

Boland, M.P., McCourt, W.J., Beate, B., 2000. Mapa geológico de la cordillera occidental del Ecuador entre 0°–1°N, escala 1/200 000. CODIGEM-Min. Energ. Min.-BGS Publs.

Bosch, D., Gabriele, P., Lapierre, H., Malfere, J.-L., Jaillard, E., 2002. Geodynamic significance of the Raspas Metamorphic Complex (SW Ecuador): geochemical and isotopic constraints. Tectonophysics 345, 83–102.

Campbell, I.H., Griffiths, R.W., 1993. The evolution of the mantle's chemical structure. Lithos 30, 389–399.

Cosma, L., Lapierre, H., Jaillard, E., Laubacher, G., Bosch, D., Desmet, A., Mamberti, M., Gabriele, P., 1998. Pétrographie et géochimie des unités magmatiques de la Cordillère occidentale d'Equateur (0°30′): implications tectoniques. Bull. Soc. Géol. Fr. 169, 739–751.

Cotteccia, V., Zezza, F., 1969. The Eocene basement of the inter-Andean corridor in the Latacunga–Ambato trough (Ecuador). Geol. Appl. Idrogeol. 4, 43–46.

Donnelly, T.W. et al., 1990. History and tectonic setting of Caribbean magmatism. In: Case, J.E. (Ed.), Geol. North Am. Am. Geol. Soc., 339–374.

Dunkley, P.N., Gaibor, A., 1998. Mapa geológico de la Cordillera Occidental del Ecuador entre 2°–3°S, escala 1/200 000. CODIGEM-Min. Energ. Min.-BGS Publs., Quito.

Faucher, B., Vernet, R., Bizon, G., Bizon, J.J., Grekoff, N., Lys, M., Sigal, J., 1971. Sedimentary Formations in Ecuador. A stratigraphic and micropaleontological survey. Bureau Études Indust. Coop. Inst. Franç. Pétrole (BEICIP). 220 pp.

Feininger, T., Bristow, C.R., 1980. Cretaceous and Paleogene geologic history of coastal Ecuador. Geol. Rundsch. 3, 849–874.

Gabriele, P., Ballevre, M., Jaillard, E., Hernandez, J., 1999. Decompression at decreasing temperatures in Eclogite-facies metapellites (El Oro metamorphic complex, SW-Ecuador): a record of fast exhumation rates. Fourth ISAG, Goettingen, Germany. IRD, Paris, pp. 245–248.

Gansser, A., 1973. Facts and theories on the Andes. J. Geol. Soc. (Lond.) 129 (1), 93–131.

Goossens, P.J., Rose, W.I., 1973. Chemical composition and age determination of tholeiitic rocks in the basic igneous complex, Ecuador. Geol. Soc. Amer. Bull. 84 (3), 1043–1051.

Hart, S.R., Dunn, T., 1993. Experimental cpx/melt partitioning of 24 trace elements. Contrib. Mineral. Petrol. 113 (1), 1–8.

Hauff, F., Hoernle, K., Schminke, U., Werner, R.A., 1997. Mid-Cretaceous origin for the Galapagos hotspot: volcanological, petrological and geochemical evidence from Costa Rica oceanic crustal fragments. Geol. Rundsch. 86, 141–155.

Hughes, R.A., Bermúdez, R., Espinel, G., 1999. Mapa geológico de la Cordillera Occidental del Ecuador entre 0°–1°S, escala 1:200 000. CODIGEM-Min. Energ. Min.-BGS Publs., Quito.

Jaillard, E., Ordonez, M., Benitez, S., Berrones, G., Jimenez, N., Montenegro, G., Zambrano, I., 1995. Basin development in an accretionary, oceanic-floored fore-arc setting: southern coastal Ecuador during Late Cretaceous–late Eocene time. AAPG Mem. 62, 615–631.

Jaillard, E., Benitez, S., Mascle, G.H., 1997. Les déformations paléogènes de la zone d'avant-arc sud-équatorienne en relation avec l'évolution géodynamique. Bull. Soc. Géol. Fr. 168 (4), 403–412.

Kerr, A.C., Marriner, G.F., Arndt, N.T., Tarney, J., Nivia, A., Saunders, A.D., Duncan, R.A., 1996a. The petrogenesis of Gorgona komatiites, picrites and basalts: new field, petrographic and geochemical constraints. Lithos 37, 2–3.

Kerr, A.C., Tarney, J., Marriner, G.F., Nivia, A., Klaver, G.T., Saunders, A.D., 1996b. The geochemistry and tectonic setting of Late Cretaceous Caribbean and Colombian volcanism. J. South Am. Earth Sci. 9, 111–120.

Kerr, A.C., Marriner, G.F., Tarney, J., Nivia, A., Saunders, A.D., Thirlwall, M.F., Sinton, C.W., 1997a. Cretaceous basaltic terranes in western Colombia: elemental, chronological and Sr–Nd isotopic constraints on petrogenesis. J. Petrol. 38, 677–702.

Kerr, A.C., Tarney, J., Marriner, G.F., Nivia, A., Saunders, A.D., 1997b. The Caribbean–Colombian Cretaceous igneous province: the internal anatomy of an oceanic plateau. Geophys. Monogr. 100, 123–144.

Kerr, A.C., Tarney, J., Nivia, A., Marriner, G.F., Saunders, A.D., 1998. The internal structure of oceanic plateaus: inferences from obducted Cretaceous terranes in western Colombia and the Caribbean. Tectonophysics 292, 173–188.

Kerr, A.C., Aspen, J.A., Tarney, J., Pilatasig, L.F., 2002. The nature and provenance of accreted oceanic terranes in western Ecuador: geochemical and tectonic constraints. J. Geol. Soc. (London) 159, 577–594.

Kerr, A.C., Tarney, J., Kempton, P., Spadea, P., Nivia, A., Marriner, G., Duncan, R., in press. Pervasive mantle plume head heterogeneity: evidence from the Late Cretaceous Caribbean-Colombian Oceanic Plateau. J. Geophys. Res.

Lapierre, H., Dupuis, V., Mercier de Lepinay, B., Tardy, M., Ruiz,

J., Maury, R.C., Hernandez, J., Loubet, M., 1997. Is the lower Duarte igneous complex (Hispaniola) a remnant of the Caribbean plume-generated oceanic plateau? J. Geol. 105, 111–120.

Lapierre, H., Dupuis, V., Mercier de Lepinay, B., Bosch, D., Monie, P., Tardy, M., Maury, R.C., Hernandez, J., Polve, M., Yeghicheyan, D., Cotten, J., 1999. Late Jurassic oceanic crust and Upper Cretaceous Caribbean plateau picritic basalts exposed in the Duarte igneous complex, Hispaniola. J. Geol. 107, 193–207.

Lapierre, H., Bosch, D., Dupuis, V., Mireille, P., Maury, R.C., Hernandez, J., Monié, P., Yeghicheyan, D., Jaillard, E., Tardy M., Mercier de Lépinay, B., Mamberti, M., Desmet, A., Keller, F., Sénebier, F., 2000. Multiple plume events in the genesis of the peri-Caribbean Cretaceous oceanic plateau province. J. Geophys. Res. 105, 8403–8421.

Lebrat, M., Megard, F., Dupuy, C., Dostal, J., 1987. Geochemistry and tectonic setting of pre-collision Cretaceous and Paleogene volcanic rocks of Ecuador: with Suppl. Data 87-23. Geol. Soc. Amer. Bull. 99 (4), 569–578.

Litherland, M., Aspden, J.A., Jemielita, R.A., 1994. The metamorphic belts of Ecuador. Overseas Mem.-Br. Geol. Surv. 11 (147 pp.).

Mahoney, J.J., Storey, M., Duncan, R.A., Spencer, K.J., Pringle, M., 1993. Geochemistry and age of the Ontong Java Plateau. Geophys. Monogr. 77, 233–261.

Malone, P., Fantin, F., Rossello, E., Miller, M., 1999. Stratigraphic characterization of the Ancón Group from seismic data (Santa Elena Peninsula, Ecuador). 4th Int. Symp. And. Geodyn. ISAG, Göttingen, pp. 467–471.

Mamberti, M., 2001. Origin and evolution of two distinct Cretaceous oceanic plateau accreted in Western Ecuador (South America): petrological, geochemical and isotopic evidence. Unpublished thesis, Univ. Lausanne–Grenoble. 241 pp.

Mamberti, M., Lapierre, H., Bosch, D., Jaillard, E., Hernandez, J., Polvé, M., submitted for publication. The early cretaceous San Juan Plutonic Suite, Ecuador: a magma chamber in an oceanic plateau. Chem. Geol.

Manhès, G., Allegre, C.J., Dupré, B., Hamelin, B., 1978. Lead–lead systematics, the age and chemical evolution of the Earth in a new representation space. Open File Rep. U.S. Geol. Surv.

McCourt, W.J., Aspden, J.A., Brook, M., 1984. New geological and geochronological data from the Colombian Andes: continental growth by multiple accretion. J. Geol. Soc. (Lond.) 141, 831–845.

McCourt, W.J., Duque, P., Pilatasig, L.F., Villagómez, R., 1998. Mapa geológico de la Cordillera Occidental del Ecuador entre 1°–2°S, escala 1/200 000. CODIGEM-Min. Energ. Min.-BGS Publs., Quito.

Neal, C.R., Mahoney, J.J., Kroenke, L.W., Duncan, R.A., Petterson, M.G., 1997. The Ontong Java Plateau. Geophys. Monogr. 100, 183–216.

Ordoñez, M., 1996. Aplicaciones del estudio de microfósiles en la industria petrolera ecuatoriana. Actas VII Cong. Ecuat. Geol. Min. Petrol., 38–52.

Pichler, H., Aly, S., 1983. Neue K–Ar Alter plutonischer Gesteine in Ecuador. Z. Dtsch. Geol. Ges. 134, 495–506.

Pratt, W.T., Figueroa, J.F., Flores, B.G., 1998. Mapa geológico de la Cordillera Occidental del Ecuador entre 3°–4°S, escala 1/200 000. CODIGEM-Min. Energ. Min.-BGS Publs., Quito.

Révillon, S., Hallot, E., Arndt, N.T., Chauvel, C., Duncan, R.A., 2000a. A complex history for the Caribbean Plateau: petrology, geochemistry and geochronology of the Beata Ridge, South Hispaniola. J. Geol. 108, 641–661.

Révillon, S., Arndt, N.T., Chauvel, C., Hallot, E., 2000b. Geochemical study of ultamafic sills, Gorgona island, Colombia: plumbing system of an oceanic plateau. J. Petrol. 41, 1127–1153.

Reynaud, C., Jaillard, E., Lapierre, H., Mamberti, M., Mascle, G.H., 1999. Oceanic plateau and island arcs of southwestern Ecuador: their place in the geodynamic evolution of northwestern South America. Tectonophysics 307, 235–254.

Romero, J., 1990. Estudio estratigráphico detallado de los acantilados de Machalilla, Provincia de Manabí. Thèse Esc. Sup. Polit. Lit., Guayaquil. 259 pp.

Sen, G., Hickey-Vargas, R., Waggoner, D.G., Maurrasse, F., 1988. Geochemistry of basalts from the Dumisseau Formation, southern Haiti: implications for the origin of the Caribbean sea crust. Earth Planet. Sci. Lett. 87, 423–437.

Shimizu, H., Sangen, K., Masuda, A., 1982. Experimental study on rare earth-element partitioning in minerals formed at 20 and 20 kbar for basaltic systems. Geochem. J. 16, 107–117.

Sinton, C.W., Duncan, R.A., 1997. Nicoya Peninsula, Costa Rica: a single suite of Caribbean oceanic plateau magmas. J. Geophys. Res. 102, 15507–15520.

Sinton, C.W., Duncan, R.A., Storey, M., Lewis, J., Estrada, J.J., 1998. An oceanic flood basalt province within the Caraibbean plate. Earth Planet. Sci. Lett. 155, 221–235.

Spadea, P., Espinosa, A., 1996. Petrology and chemistry of late Cretaceous volcanic rocks from the southernmost segment of the Western Cordillera of Colombia (south America). J. South Am. Earth Sci. 9, 79–90.

Sun, S.S., McDonough, W.F., 1989. Chemical and isotopic systematics of oceanic basalts: implications for mantle composition and processes. Geol. Soc. Spec. Publ. 42, 313–345.

Toussaint, J.-F., Restrepo, J.J., 1994. The Colombian Andes during Cretaceous times. In: Salfity, J.A. (Ed.), Cretaceous Tectonics in the Andes. Earth Evolution Sciences, Vieweg, Braunschweig, pp. 61–100.

Ulmer, P., 1989. Partitioning of high field strengh elements among olivine, pyroxenes, garnet and calcalkaline picrobasalt: experimental results and an application. Annu. Rep. Dir. Geophys. Lab. 1988/89, 42–47.

White, W.M., Hofmann, A.W., Puchelt, H., 1987. Isotope geochemistry of Pacific mid-ocean ridge basalt. J. Geophys. Res. 92, 4881–4893.

Zindler, A., Hart, S., 1986. Chemical geodynamics. Annu. Rev. Earth Planet. Sci. Lett. 14, 493–571.